Journal of Geophysical Research: Oceans

RESEARCH ARTICLE
10.1029/2018JC014017

Influences of the Kuroshio on Interisland Remote Connectivity of Corals Across the Nansei Archipelago in the East China Sea

Yusuke Uchiyama[1,2], Sachika Odani[1], Motohiko Kashima[3], Yuki Kamidaira[4,1], and Satoshi Mitarai[5]

[1]Department of Civil Engineering, Kobe University, Kobe, Japan, [2]Coastal and Estuarine Environment Department, Port and Airport Research Institute, Yokosuka, Japan, [3]Department of Humanities, Kobe Gakuin University, Kobe, Japan, [4]Nuclear Science and Engineering Center, Japan Atomic Energy Agency, Tokai, Japan, [5]Marine Biology Unit, Okinawa Institute of Science and Technology, Onna, Japan

Key Points:
- Dispersal of coral spawn and larvae is investigated using double-nested circulation modeling coupled with a Lagrangian particle tracking model
- Corals mostly remain near the release areas, while a nontrivial portion is transported ~1,000 km over the archipelago due to the Kuroshio
- Corals are partly separated from the Kuroshio, entrained in the Kuroshio Counter Current, and transported eastward to Okinawa Island

Supporting Information:
- Supporting Information S1
- Data Set S1
- Data Set S2
- Data Set S3
- Data Set S4
- Data Set S5
- Data Set S6
- Data Set S7
- Data Set S8
- Data Set S9
- Data Set S10
- Data Set S11
- Data Set S12
- Data Set S13
- Data Set S14

Correspondence to:
Y. Uchiyama,
uchiyama@harbor.kobe-u.ac.jp

Citation:
Uchiyama, Y., Odani, S., Kashima, M., Kamidaira, Y., & Mitarai, S. (2018). Influences of the Kuroshio on interisland remote connectivity of corals across the Nansei Archipelago in the East China Sea. *Journal of Geophysical Research: Oceans*, *123*, 9245–9265. https://doi.org/10.1029/2018JC014017

Received 27 MAR 2018
Accepted 27 NOV 2018
Accepted article online 29 NOV 2018
Published online 25 DEC 2018

Abstract For the preservation and protection of coral habitats along the Nansei Archipelago in the East China Sea, a submesoscale eddy-resolving synoptic ocean model was developed based on the Regional Oceanic Modeling System coupled with a 3-D Lagrangian particle tracking model. Millions of neutrally buoyant particles representing coral spawn and larvae were released from 19 major islands and one lagoon every spring from 2012 to 2015. The model results were compared to satellite data, in situ observation, and surface drifters to confirm reasonable agreement. The connectivity matrix across the archipelago was quantified using Lagrangian probability density functions of the modeled particle displacement. Most particles remained near the release areas, while some traveled long distances by the northeastward drifting Kuroshio, leading to notable interisland coral transport across the archipelago that promotes *interisland connectivity*. A possible mechanism was examined by analyzing the transition from coastal to pelagic transport of the particles released from the Yaeyama Islands, the southernmost area of the archipelago. The Kuroshio trapped the particles released from the northern coast of the islands with considerable temporal variability in the entrainment rate. By contrast, particles released from the southern coast are markedly affected by the eastward current around the release sites, which significantly reduces their entrainment in the Kuroshio and, thus, long-distance transport. Some entrained particles were expelled abruptly from the Kuroshio, trapped by the southwestward drifting Kuroshio Counter Current developed between the Kuroshio and the archipelago, and subsequently transported eastward to the islands.

Plain Language Summary For the preservation and protection of coral habitats along the Nansei Archipelago in the East China Sea, we conducted 3-D tracking of particles mimicking coral spawn and larvae released from shallow seas around the islands across the Nansei Archipelago, based on a numerical 3-D ocean circulation model, Regional Oceanic Modeling System. Although the released corals were mostly transported short distances and settled down near the release sites, a moderate amount was entrained in the northeastward drifting Kuroshio Current developed in ~150 km west of the islands. The entrained particles could be conveyed northeastward for ~1,000 km, leading to interisland population connections. However, the entrainment rate largely depended on locations of the releases and variability in local oceanic currents upon the releases. Furthermore, some entrained particles were expelled abruptly from the Kuroshio, trapped by the southwestward drifting Kuroshio Counter Current developed between the Kuroshio and the archipelago, and subsequently transported eastward to the islands. These findings can be directly utilized in policy-making for the effective design management of marine protected areas.

1. Introduction

Coral reefs are among the most biologically diverse and productive marine ecosystems on the globe (cf., Connell, 1978), playing important roles in many aspects. For instance, coral reefs host favorable habitat to an extensive variety of flora and fauna and are home to ~25% of marine life in the world's oceans, while providing favorable conditions for the evolution of new species (Paulay, 1997). These reefs serve as remarkably effective wave absorbers that protect shorelines from severe storms and erosion. Moreover, coral reefs also support the regional economy and tourism as a recreation resource (e.g., Moberg & Folke, 1999). However, because of overharvesting, pollution, disease, and climate changes, corals worldwide have recently been

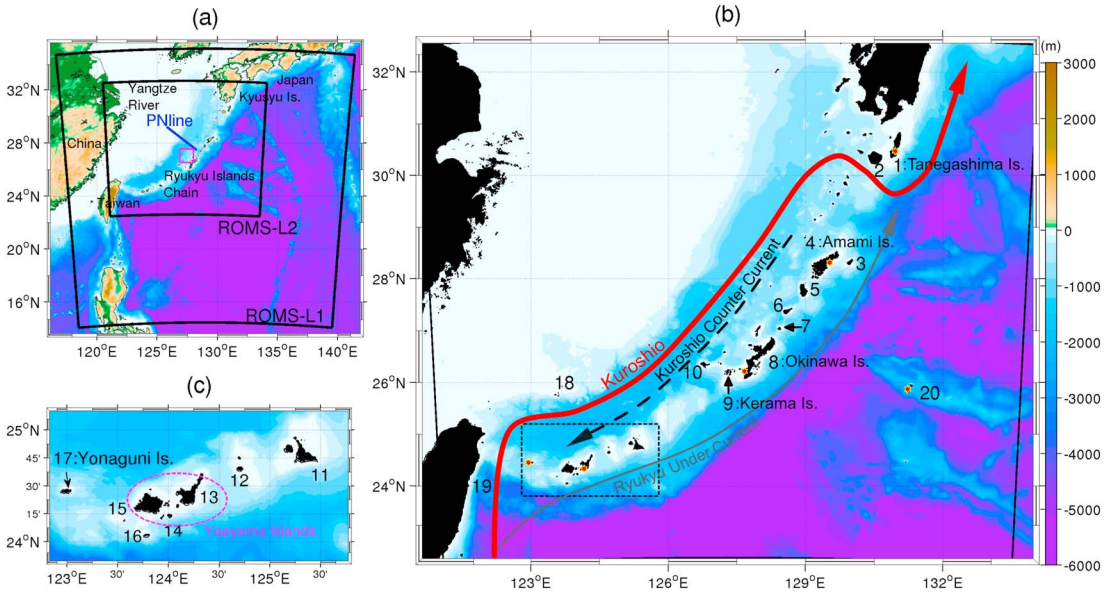

Figure 1. (a) ROMS-L1 and L2 model domain and bathymetry (m) in color. Blue line indicates the PN-line transect of the Japan Meteorological Agency (JMA) used for Figure 3. A magenta box represents the domain for the wavenumber kinetic energy spectral analysis in Figure 13. (b) An enlarged figure of (a) approximately coinciding with the ROMS-L2 domain that encompasses the entire chain of the Nansei archipelago. Red stars depict the locations of tide gauge stations used for the harmonic analysis in Figure 4. The arrows represent approximate paths of the three major currents around the study area. Red: Kuroshio, gray: Ryukyu under current, dashed black: Kuroshio Counter Current, respectively. (c) The inset corresponds to the Yaeyama Islands area bounded by the broken rectangular in (b). The numbers identify the 20 selected major areas (19 islands and one lagoon) for the source and sink sites used in the costal connectivity matrix quantification. The full list of the names of these areas is presented in Table 1 and Figure 5b.

threatened by a considerable decline in biomass (Bellwood et al., 2004). The reasons behind this downward trend include the high sensitivity of corals to their surroundings. Factors, such as water temperature, salinity, and light for photosynthesis, are widely known as principal factors that effect on coral growth (Hoegh-Guldberg, 1999). Corals generally inhabit ecosystems with a salinity range between 32 and 40 psu and a rapid decrease in salinity brings death to corals (Hoegh-Guldberg & Smith, 1989; Veron, 1986). Light also plays a major role in providing the energy for driving photosynthetic activity of zooxanthellae (Chalker et al., 1988), a symbiotic alga that is also particularly sensitive to high turbidity in near-surface waters. Finally, corals require water temperatures in a relatively narrow range, typically between 18 and 30 °C, resulting in a general restriction of their habitable latitude band between 30°N and 30°S (e.g., Hoegh-Guldberg, 1999).

The Nansei Archipelago, commonly known as the Ryukyu Islands, is a chain of islands that stretch northeast between Taiwan and Kyushu (Figure 1 and Table 1). The islands are in the subtropical region of Japan, hosting ecologically abundant coral reefs, even though they are situated at the northernmost extreme of the habitable region. The Kuroshio plays a key role in heat transport from the lower latitudes, and maintains warm water temperatures adequate for the growth of corals. The Kuroshio is one of the most powerful western boundary currents generated from the North Pacific Subtropical Gyre, originating near the Philippines. The current enters the East China Sea (ECS) through the passage located between the east coast of Taiwan and Yonaguni Islands (#17; Figure 1c), the southernmost island of the archipelago (Figure 1b), and drifts northeastward along the continental shelf slope in the central ECS at a mean net volume transport of 18.7 to 23.0 Sv (e.g., Andres et al., 2008; Ichikawa & Beardsley, 1993; Ichikawa & Chaen, 2000; Johns et al., 2001). The Kuroshio's intensive poleward transport of warm water extends the northern limit of coral habitats to much higher latitudes along the Kuroshio path, for example, to Tanegashima Islands (#1; Figure 1b) at 30.574°N, the northernmost major island in the archipelago, compared to other parts of the world's oceans (Ikeda et al., 2006).

Three mechanisms are anticipated to promote transverse, southeastward transport of warm water from the Kuroshio to the coastal areas around the Nansei Archipelago situated ~150 km from the Kuroshio

Table 1
The Names, Geographical Positions, and the Number of Patches of the 19 Selected Major Islands and a Lagoon Are Shown in Figures 1b and 1c

Site Number	Name	Latitude	Longitude	Number of Patches
1	Tanegashima Island	30°37′28″	130°59′46″	14
2	Yakushima Island	30°20′46″	130°31′14″	11
3	Kikaijima Island	28°19′22″	129°58′25″	6
4	Amamioshima Island	28°22′38″	129°29′38″	20
5	Tokunoshima Island	27°47′21″	128°58′29″	9
6	Okinoerabujima Island	27°22′43″	128°36′43″	8
7	Yoronshima Island	27°02′40″	128°25′59″	4
8	Okinawa Island	26°13′12″	127°42′08″	40
9	Kerama Islands[*1]	26°10′36″	127°21′11″	7
10	Kume Island	26°20′29″	126°47′15″	6
11	Miyako Island	24°47′26″	125°18′12″	11
12	Tarama Island	24°39′33″	124°42′00″	6
13	Ishigaki Island	24°20′18″	123°58′40″	14
14	Sekisei Lagoon[*2]	24°24′55″	124°12′14″	5
15	Iriomote Island	24°20′34″	123°48′48″	8
16	Hateruma Island	24°03′24″	123°46′52″	3
17	Yonaguni Island	24°27′18″	122°59′16″	4
18	Senkaku Islands[*3]	25°44′44″	123°28′27″	4
19	Taiwan	23°52′42″	120°57′24″	38
20	Daito Islands[*4]	25°50′43″	131°14′33″	6

Note. The patches surrounding these islands and lagoon are used as the source and sink sites of Lagrangian particles for the coastal connectivity analysis. Asterisks identify local archipelagos, where the positions are indicated by those of (1) Tokashiki Islands, (2) Kohama Islands, (3) Utsurijima Islands, and (4) Minamidaito Islands, respectively.

axis. First, there is a quasi-persistent intrusion of the Kuroshio due to mesoscale and submesoscale eddy-induced lateral mixing (Kamidaira et al., 2017). The second mechanism is the direct advective influence from the Ryukyu Under Current (RUC), a branch current of the Kuroshio running along the eastern side of the Nansei Archipelago. The RUC is a subsurface current, which is split from the Kuroshio east of Taiwan and merges with the Kuroshio again north of Amamioshima Island (e.g., Ichikawa et al., 2004; Yuan et al., 1998), carrying warm water from the lower latitudes to the east coast of the archipelago. Although the RUC is largely responsible for poleward heat transport, its contribution to the maintenance of marine ecosystem in the Nansei Archipelago is not substantial because the RUC's main body is situated at ~600 m below the surface (Ichikawa et al., 2004) where larvae and spawn of marine fauna are rare. The third mechanism is due to the transverse advective effects associated with the Kuroshio Counter Current, which often develops between the archipelago and the Kuroshio (e.g., Hisaki & Imadu, 2009; Ichikawa & Beardsley, 2002; Qiu & Imasato, 1990, and references therein). The KCC manifests as a quasi-persistent southwestward current with pronounced appearance of mesoscale eddies, extracting water from the Kuroshio, and transporting it toward the west coast of the archipelago. This is an important mechanism that dynamically connects the Kuroshio with the islands, which are typically separated by approximately 100–200 km (cf., the distance between the Kuroshio and Okinawa (Main) Island is ~150 km). This suggests that the Kuroshio and the KCC concurrently promote the transport and dispersal of coral spawn and larvae across the islands.

Nevertheless, the corals in the Nansei Archipelago have suffered severely from occasional coral bleaching since the most intensive bleaching event in 1998, which affected coral ecosystems worldwide. Priority should be given to those coral reefs that have a healthy and reliable supply of spawn. Therefore, specifying the origin of the coral spawn supply is an essential consideration to properly identify those coral ecosystems that should be given the highest priority (e.g., Munday et al., 2009). In doing so, connectivity of coral spawn and larvae will inevitably play an important role in the development of policies that effectively identify and manage marine protected areas.

Genetic markers and numerical models have generally been used to measure coastal connectivity associated with nearshore and pelagic dispersal of coral spawn and larvae. For instance, Wood et al. (2014)

estimated a connectivity of virtual coral larvae by using the global ocean circulation product based on a 1/12° HYCOM reanalysis product (Chassignet et al., 2007) coupled with a Lagrangian particle tracking model for the domain between 47°N and 47°S, reporting that the northeastward larval transport prevails along the Kuroshio around the Nansei Archipelago. Nakajima et al. (2010) confirmed this observation using a population genetic approach based on the genetic connectivity of *Acropora digitifera*, which is one of the common coral species in the Nansei Archipelago, extending across a large geographic area inclusive of the seven major regions (Kerama, Miyako, Ishigaki, Tanegashima, Amamioshima, and Okinawa Islands and Sekisei Lagoon) along the 1,000-km-long chain of the islands. Nakajima et al. (2010) also suggested that *A. digitifera* populations in the Nansei Archipelago may be able to recover rapidly if the coral ecosystem is properly maintained and managed, with other reefal systems serving as the spawn and larval source.

Extensive field campaigns have been carried out in several individual islands and specific local coral reefs in the Nansei Archipelago to characterize local spawn transport mechanisms (e.g., Nakamura et al., 2017; Yamano et al., 1998). To date, some efforts have already been made by combining in situ measurement and local numerical circulation modeling to analyze influences of ambient currents on coral spawn dispersal (e.g., Shimokawa et al., 2014; Tamura et al., 2007). There is a growing consensus of opinion among experts that complicated coastal currents on complex reefal bathymetries could significantly alter the oceanic coral transport and dispersal, in particular for their initial behavior just after release (viz., spawning). Accordingly, the demand for high-resolution numerical modeling has been on the rise so that complex coastal topography can be adequately defined while encompassing a sufficiently extensive domain to illustrate interisland and much longer transport distances induced by the Kuroshio.

Based on the above arguments, the primary objective of this study was to quantify coastal connectivity of coral spawn and larvae across the islands using a state-of-the-art, high-resolution, coupled numerical hydrodynamic and particle tracking model. Particular attention was paid to interisland, remote connectivity, primarily induced by the Kuroshio, which persistently drifts northeastward on the continental shelf break of the ECS. The circulation model was expected to adequately account for multiscale physics comprising synoptic-scale currents (viz., the Kuroshio, KCC, RUC), mesoscale and submesoscale eddies, and nearshore flows influenced by complex coastal topography and bathymetry, all of which are anticipated to be responsible for fate of coral larvae. A high-resolution model is required for accurate evaluation of detachment and settlement of larvae in shallow areas, referred to as "nearshore retention," as has been argued in the previous modeling studies (e.g., Wolanski & Kingsford, 2014). An Eulerian passive tracer transport model in our own previous work (Kamidaira et al., 2018) has also demonstrated that high-resolution models are inevitable to obtain a plausible reproducibility of concentration field confined near the coasts, and that a 1-km lateral grid spacing is a marginally sufficient resolution. Moreover, a massive amount of Lagrangian particles representing planktonic coral larvae by considering their spawning timing and depth and survival rate before settlement was released from nearshore sites across the archipelago to properly quantify long-distance larval transport that scarcely occurs. The modeled ambient 3-D currents were exploited to trace the released larvae (particles) and to evaluate population connectivity based on Lagrangian probability density function estimated from particle tracking experiments. To this end, a double nested high-resolution synoptic ocean model with Regional Oceanic Modeling System (ROMS; Shchepetkin & McWilliams, 2005, 2008) was developed with grid spacing down to 1 km. This ROMS model was coupled with an off-line 3-D Lagrangian particle tracking model over a sizable area embracing all the major islands in the archipelago. The computational period of the particle tracking was chosen for spring to represent coral spawning for a four-year period between 2012 and 2015.

The remainder of this paper is organized as follows. The modeling framework used for the hindcast experiment and the method to quantify connectivity based on Lagrangian probability density functions (PDFs) of the modeled particle displacement are described in section 2. Section 3 demonstrates the model's reproducibility through extensive comparisons with in situ observations and satellite altimetry data from an Eulerian viewpoint. The pelagic interisland connectivity across major islands and a lagoon in the Nansei Archipelago are presented in section 4. In section 5, influences of the Kuroshio on long-distance transport and spatially extensive dispersal of emulated corals responsible for interisland connectivity are examined. In section 6, we examined particles that are entrained in the Kuroshio, travel long distance, and then are abruptly separated from the Kuroshio to approach Okinawa Island due to the KCC and associated eddy mixing. Finally,

conclusions as well as discussion on comparison with other sites including the Great Barrier Reef, Australia, and the Florida Keys, USA, are presented in section 7.

2. The Models

2.1. Japan Coastal Ocean Predictability Experiment Version 2–ROMS Downscaling Circulation Model

Figure 1 shows the numerical domain of the oceanic downscaling model in a double-nested configuration embedded in the Japan Coastal Ocean Predictability Experiment version 2 (JCOPE2; Miyazawa et al., 2009) domain. JCOPE2 is a numerical reanalysis product for the northwestern Pacific Ocean assimilated with a vast amount of satellite and in situ data, including Argo floats using three-dimensional variational assimilation. The JCOPE2 product is provided as daily-averaged sea surface height (SSH), temperature, salinity, and meridional and zonal horizontal current velocities, which are spatiotemporally projected onto the perimeter of the ROMS-L1 model for the open boundary conditions. The one-way off-line nesting approach described in Mason et al. (2010), Uchiyama et al. (2014), Uchiyama, McWilliams, et al. (2017), Uchiyama, Suzue, et al. (2017), Uchiyama, Kanki, et al. (2017), Uchiyama et al. (2018), Kamidaira et al. (2017, 2018), and Tada et al. (2018) is applied to successively decreasing grid spacing from ~10 km (JCOPE2) to 3 km (ROMS-L1), and further down to 1 km (ROMS-L2). The parent ROMS-L1 model is designed to encompass a wide area to account for the Kuroshio flowing from the Taiwan Strait, consisting of 768 × 768 horizontal grid cells and 32 vertically stretched terrain- and surface-following *s* layers (Shchepetkin & McWilliams, 2005). The innermost ROMS-L2 model has 1,280 × 1,120 cells laterally and 32 *s* layers vertically, covering the whole chain of the Nansei Archipelago from the northeastern part of Taiwan to the southern tip of Kyusyu (Figures 1a and 1b).

The model topography was obtained from the Shuttle Radar Topography Mission at 30-arc-sec resolution (SRTM30_Plus; Rodríguez et al., 2005; Becker et al., 2009), which covers the global ocean at 30 geographic arc seconds, supplemented by the Japan Oceanographic Data Center-Expert Grid data for Geography at 500-m resolution (http://www.jodc.go.jp/jodcweb/JDOSS/infoJEGG.html) for the coastal region around Japan. Surface wind stresses were obtained from the QuickSCAT-ECMWF blended wind data (e.g., Bentamy et al., 2007) for 2005–2007 and the Grid Point Values Global Spectral Model operational atmospheric product from the Japan Meteorological Agency (JMA) with horizontal resolution of 0.2° × 0.25° for 2008–2015. Net heat, freshwater, and radiation fluxes at the ocean surface were obtained from the NOAA Comprehensive Ocean–Atmosphere Data Set (Woodruff et al., 1987) monthly climatology. The 20-day averaged JCOPE2 data were applied to sea surface temperature and salinity restoration with a nudging time scale of 90 days to correct long-term biases caused by the imposed climatological Comprehensive Ocean–Atmosphere Data Set surface fluxes. The monthly climatology of the major river discharges in Dai et al. (2009) was applied for Yangtze River as an additional surface freshwater flux distributed around the river mouth. To improve the reproducibility of the Kuroshio, we introduced a four-dimensional nudging for temperature and salinity with a weak nudging inverse time scale of 1/20 days toward the 10-day averaged JCOPE2 3-D temperature and salinity fields (Uchiyama, McWilliams, et al., 2017). This combination of the data sets and configuration has been exploited for high-resolution modeling of the Kuroshio around Japan extensively with great successes (e.g., Tada et al., 2018; Uchiyama, McWilliams, et al., 2017; Uchiyama, Suzue, et al., 2017). For further details of the present ROMS-L1 model configuration, readers should refer to Kamidaira et al. (2017).

The child ROMS-L2 model was initialized and forced along the perimeter by the spatiotemporally interpolated daily-averaged ROMS-L1 output. The hourly output of the JMA GPV-Meso Scale Model operational atmospheric reanalysis with horizontal resolution of 0.05° × 0.0625° was utilized for the ROMS-L2 model instead of the Grid Point Values Global Spectral Model used for the L1 model. The same sea surface temperature and sea surface salinity restoration for the surface flux correction was included as was done for the L1 model. Ten principal tidal constituents from the TPXO.7.0 global tidal reanalysis (Egbert et al., 1994; Egbert & Erofeeva, 2002) were additionally imposed on the SSH along the perimeter to include barotropic tides and resultant intrinsic baroclinic tides. The temperature and salinity nudging was not applied to the L2 model, so as not to interfere with spontaneous development and decay of intrinsic eddies. A computational period of approximately six years was chosen for the ROMS-L2 model from December 2010 to November 2015. The other numerical conditions were the same as those used in the ROMS-L1 model configuration as summarized in Table 2.

Table 2
Computational Configurations for the ROMS-L1 and ROMS-L2 Models

	ROMS-L1	ROMS-L2
Computational period	1/1/2005–2/11/2015	27/12/2010–2/11/2015
Grid cells	768 × 768 (×32 layers)	1280 × 1120 (×32 layers)
Horizontal grid resolution	3.0 km	1.0 km
Baroclinic time step	240 s	40 s
Surface wind stress	QuikSCAT-ECMWF (daily, till 31/12/2007)	JMA GPV-MSM (hourly)
	JMA GPV-GSM (daily, 1/1/2008, and later)	
Surface flux	NOAA COADS (monthly climatology)	
SST and SSS to restore	JCOPE2 (20-day averaged)	
Yangtze River discharge	Monthly climatology (Dai et al., 2009)	
Open boundary/initial conditions	JCOPE2 (daily)	ROMS-L1 (daily)
TS nudging	JCOPE2 (10-day averaged)	-
Tides	-	TPXO 7.0
Topography	SIO SRTM30_Plus	

2.2. Offline Lagrangian Particle Tracking Model

Coastal connectivity around the Nansei Archipelago was estimated from Lagrangian probability functions (PDFs) with an enormous amount of Lagrangian particles originating from arbitrary nearshore sites around major islands and a lagoon where spawn and larvae are released. We exploited the off-line 3-D Lagrangian particle tracking model developed in Carr et al. (2008) and used previously, for example, in Mitarai et al. (2009) and Romero et al. (2013) with the ROMS model outputs. This off-line model integrates the Lagrangian equation of motion of the *n*th realization of fluid particle,

$$\frac{\partial}{\partial \tau}\boldsymbol{X}_n(\tau,\boldsymbol{a}) = \boldsymbol{U}_n(\tau,\boldsymbol{a}), \tag{1}$$

where $\boldsymbol{U}_n(\tau,\boldsymbol{a})$ and $\boldsymbol{X}_n$, respectively, indicate the velocity and position of the *n*th Lagrangian particle; $\boldsymbol{a}$ is the initial position of the particle of interest; and τ is the elapsed time, usually referred to as advection time. Note that variables in bold denote vectors. The particle velocity $\boldsymbol{U}_n$ is expressed by

$$\boldsymbol{U}_n(\tau,\boldsymbol{a}) = \boldsymbol{u}[\boldsymbol{X}_n(\tau,\boldsymbol{a}), t_n + \tau], \tag{2}$$

where $\boldsymbol{u}(\boldsymbol{x}, t)$ is the Eulerian velocity at a given location $\boldsymbol{x}$ and time t and t_n indicates the release time of the *n*th Lagrangian particle. The Eulerian velocity at a given particle location is estimated through liner interpolation in time and space of the discrete velocity fields. A fourth-order accurate Adams-Bashforth-Moulton predictor–corrector scheme is employed over time for solving equations (1) and (2) with a series $\boldsymbol{u}$ of stored 2-hr-averaged 3-D ROMS velocity. Hence, the particle tracking model is capable of simulating the trajectories of many Lagrangian particles released from arbitrary nearshore sites defined around the Nansei Archipelago, once the ROMS-L2 circulation field is obtained.

Our coupled model takes into account basic biological properties of coral species in the area, dominated by *Acropora* (e.g., *A. tenuis* and *A. hyacinthus*). After spawning, coral eggs evolve into zooplanktons (planula larva) in several days, which have weak swimming ability that we omitted merely for the simplicity in the modeling. Hayward et al. (2011) reported that *Acropora*'s egg is buoyant to reach near the surface, yet they spawn in depths of 8–20 m. We assumed that eggs are released near the surface, at 3 m below the surface to formally avoid influences from a thin surface Ekman boundary layer. In general, planula larvae of corals survive a few days to a few months before settlement. Marine biologists have introduced a concept of "50% survival rate" to interpret whether larvae successfully settle down their favorable nearshore areas to grow into adults. Nishikawa et al. (2003) and Nozawa and Okubo (2011) have reported that 50% survival rate of *Acropora* in the study area is 21–25 days. Therefore, we employed 21 days as the maximum advection time to trace Lagrangian particles. In the present particle tracking model, released particles were tracked with a time step of 200 s for at least 21 days, or until they crossed the boundaries of the L2 model domain, or were beached on a land grid. The estimated total number of Lagrangian particles, release dates of particles, and positions of sink and source areas are detailed in sections 4.1 and 5.1, respectively. We did not introduce any ad hoc

behavior models, such as random walk subgrid-scale diffusivity or diel vertical migration, to avoid further complexity and uncertainty. These factors should be examined in future works.

2.3. Lagrangian PDF and Coastal Connectivity

To quantify the dispersal of Lagrangian particles released from source patches, we calculate Lagrangian PDFs following the methodology described in Mitarai et al. (2009) from the results of the particle tracking model. A Lagrangian PDF represents the probability density function of particle displacement for a given advection time τ. Its discrete representation is

$$f_x'(\xi;\tau,\boldsymbol{a}) = \frac{1}{N}\Sigma_{n=1}^{N}\delta(\boldsymbol{X}_n(\tau,\boldsymbol{a}) - \xi), \tag{3}$$

where N is the total number of Lagrangian particles, δ is the Dirac delta function, and ξ is the sample space variable for $\boldsymbol{X}$. Although tracking is conducted three-dimensionally, the results are illustrated in a horizontal two-dimensional format; thus, $f_x'(\xi;\tau,\boldsymbol{a})$ is evaluated only in the horizontal directions, primarily because the particles generally remain in the upper ocean. Discrete Lagrangian PDFs are evaluated from the center location of the release sites defined later, averaged over each site. Hence,

$$f_x'(\xi;\tau,\boldsymbol{a}) \approx \frac{1}{\pi R^2}\int_{|r|\le R} f_x'(\xi;\tau,\boldsymbol{a}+\boldsymbol{r})d\boldsymbol{r}, \tag{4}$$

where R is the radius of each release site $\boldsymbol{a}$ defined later. The final form of discrete Lagrangian PDF is obtained after applying an isotropic spatial Gaussian filter $G(\boldsymbol{x}-\xi)$ with standard deviation of 3 km:

$$f_x(\xi;\tau,\boldsymbol{a}) \approx \int_{-\infty}^{\infty} G(\boldsymbol{x}-\xi) f_x'(\xi;\tau,\boldsymbol{a})d\boldsymbol{x}. \tag{5}$$

Coastal connectivity, denoted by $C_{ji}(\tau)$ here, is defined as the probability of Lagrangian fluid particles transported from a source site j to a sink site i over a time interval τ.

$$C_{ji}(\tau) = f_x\left(\xi = \boldsymbol{x}_i;\tau,\boldsymbol{a} = \boldsymbol{x}_j\right)\left(\pi R^2\right), \tag{6}$$

where $\boldsymbol{x}_j$and $\boldsymbol{x}_i$ are the source and sink patch locations, and the normalization by πR^2 converts the PDFs to probabilities. For further details on mathematical representations and their physical interpretations, readers should refer to Mitarai et al. (2009).

The Lagrangian analyses were performed for the particles positioned at all the depths for quantitative measures of the total transport rather than near-surface transport. We observed that long-distance transport occurs near the surface, where currents are most energetic. The coupled model result indicated that particles mostly stay in the upper ocean, despite their substantial three-dimensional behavior. Our preliminary inspection of comparison between the near-surface Lagrangian transport and depth-integrated transport exhibited that they are qualitatively equivalent. Therefore, we decided that the depth-integrated results are demonstrated in the present study.

3. Model Validations

In this section, the newly developed ROMS-L2 model is validated with satellite and in situ observations and the assimilative JCOPE2 reanalysis. It is worth noting that Kamidaira et al. (2017) has already demonstrated good agreement between similar double-nested ROMS-L1 and L2 results and the corresponding observations over a 2.5-year period from 2010 to 2013. To validate reproducibility in the mean structure and variability of synoptic-scale and mesoscale motions near the ocean surface, the present L2 model output was compared with the satellite altimetry data produced and distributed by the Archiving, Validation, and Interpretation of Satellite Oceanographic (AVISO) data (e.g., Le Traon et al., 1998). In particular, we utilized the AVISO Ssalto/Duacs gridded multimission altimeter products, that is, the gridded data sets of daily SSH anomaly and associated geostrophic velocity composite at 1/4° resolution. Additionally, surface velocity and SSH of the assimilative JCOPE2 reanalysis are used for a further confirmation.

Figure 2 shows time-averaged surface currents and temporal variances of SSH for the entire one year of 2012 from the three outcomes, viz., the AVISO, JCOPE2, and ROMS-L2 embedded in the ROMS-L1 output. The SSH

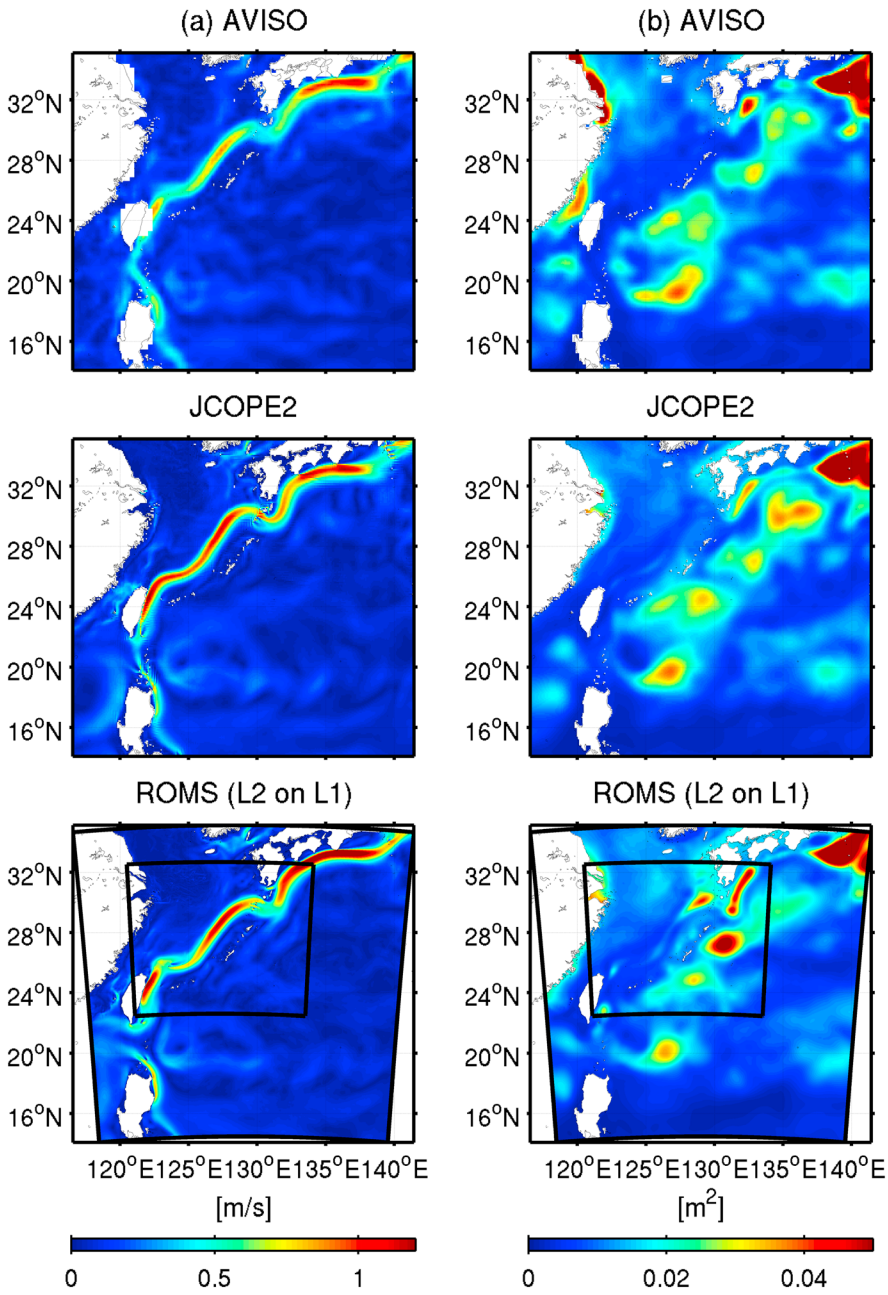

Figure 2. Plan view plots of (a) the time-averaged surface velocity magnitude (left column) and (b) temporal variance of SSH (right column) for the entire year 2012. From top to bottom panels, the results from the AVISO satellite altimetry data, JCOPE2, and ROMS-L2 (embedded in the L1 results) are depicted.

variances represent synoptic and mesoscale variability at the surface due to the transient Kuroshio path and resolved eddies. The modeled mean Kuroshio path represented by larger geostrophic surface current velocity (warm colors) of the ROMS models is consistent with that of the AVISO and JCOPE2, particularly in the ECS (Figure 2a). The ROMS-derived SSH valiance exhibits several important features with magnitudes equivalent to those obtained from the AVISO data (Figure 2b). For example, smaller variances are observed on the persistent Kuroshio path on the western side of the archipelago in the ECS as compared with those on the eastern side. More intensive eddy activity in the east of the archipelago is apparently caused by influences of westward propagating mesoscale eddies as Rossby waves headed toward the eastern side of the chain of the islands (e.g., Liu et al., 2012; Qin et al., 2015). In contrast, the other high SSH variances south of Kyushu and in the Kuroshio Extension Region (cf., Kamidaira et al., 2018; Uchiyama, Suzue, et al.,

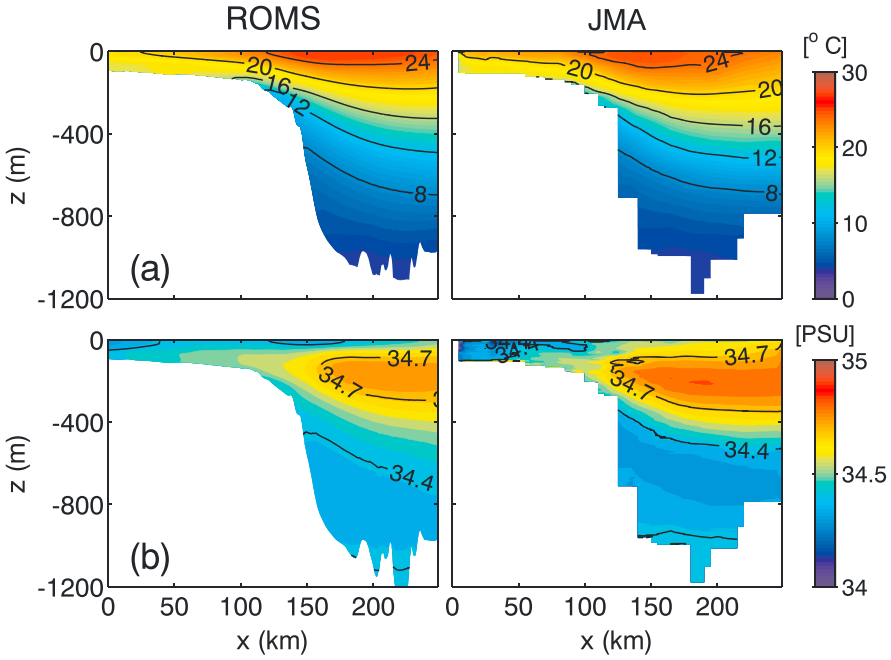

Figure 3. (a) Seasonally averaged temperature and (b) salinity for spring from (left) the ROMS-L2 model and (right) the JMA observations in the vertical section along the PN line (Figure 1a).

2017) correspond to the areas where the Kuroshio path largely meanders, reflecting intrinsic synoptic variability of the Kuroshio.

The modeled stratification was then compared with repeated in situ hydrographic observations in the vertical section along the PN line transect performed by JMA, shown by the blue line in Figure 1a. The measurements along the PN line comprise 16 conductivity, temperature, and depth casts that have been obtained seasonally since 1972 to date from JMA's research vessels. Figure 3 is an example that shows comparisons of the seasonally averaged temperature (Figure 3a) and salinity (Figure 3b) for spring from April to June for the entire model years, when coral spawning mostly occurs in the study area (section 4.1). It is clearly exhibited that the modeled seasonal climatology of the stratification shows a good agreement with the observation, not only in spring but also in all the four seasons (not shown).

Subsequently, Figure 4 shows the result of a harmonic analysis of surface elevations from ROMS-L2 and in situ tidal observations at six tide gauge stations of JMA in Daito Islands, Tanegashima Islands, Amamioshima Islands, Okinawa Islands, Ishigaki Islands, and Yonaguni Islands, shown by the red markers in Figure 1b. The tidal harmonic analysis was conducted with the data from 1 January to 31 December in 2013. We show the result for four selected principal tidal constituents (M_2, S_2, K_1, and O_1) as scatterplots of amplitudes and phase epochs of the four components. The tidal amplitude and phases are reasonably well reproduced by the L2 model with the correlation coefficients of 0.997 and 0.990, respectively, whereas the M_2 lunar semidiurnal amplitudes were slightly underestimated in approximately 10–20% of those of the observation, presumably due to underresolved topographic influences near the gauges. The evidence described above suggests that the present ROMS-L2 model is sufficiently capable of reproducing the synoptic and mesoscale features including those due to the Kuroshio, as well as high-frequency tidal variability around the Nansei Archipelago.

4. Coastal Connectivity Across the Archipelago

4.1. Particle Tracking Experiment 1

For quantification of costal connectivity across the Nansei Archipelago, we performed a 3-D Lagrangian particle tracking experiment (experiment 1) using the ROMS-L2 3-D flow field at 2-hr intervals. The configuration of experiment 1 is summarized in Table 3. A total of 19 major islands and a lagoon were chosen as source and

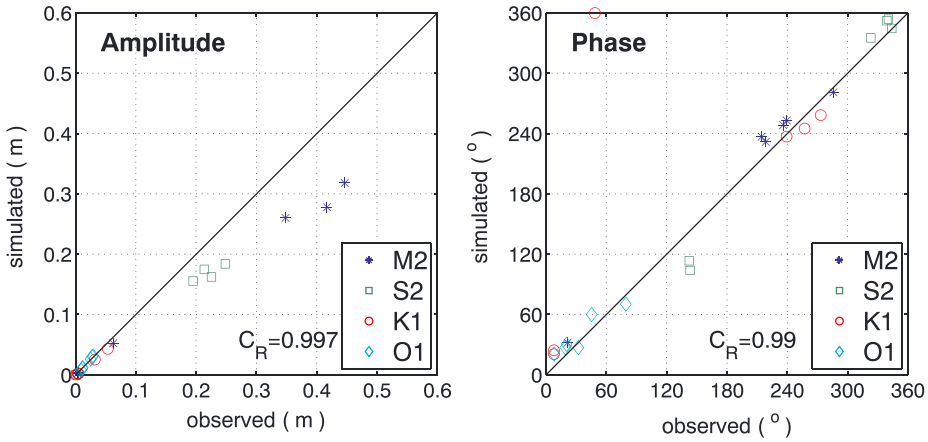

Figure 4. Scatter diagram of four principal tidal constituents (M_2, S_2, K_1, and O_1) derived from a harmonic analysis of the hourly surface elevations from ROMS-L2 and observation at six tide gauge locations of JMA in the Nansei Archipelago depicted in Figure 1b. (a) Amplitudes and (b) phase epochs. C_R in each plot indicates the correlation coefficient.

sink sites of corals (Figure 1b). Relatively small circular areas, which we call source/sink patches, with a diameter of 10 km are defined next to the shorelines to surround each of the 20 sites with minimal gaps between them, comprising a total of 224 patches in the L2 domain. About 1.5 million Lagrangian particles were released at 3 m below the surface (section 2.2). To be consistent with the life cycle of corals, these particles were tracked for up to 21 days after the release, until they were beached on land grids, or until they exited the L2 domain through the open boundaries.

Spring was chosen for the experiments because it is the season when coral spawning and subsequent larval transport occur in the Nansei Archipelago. The dominated reefal corals in the study area, *Acropora*, are well known to spawn synchronously at one particular night in May or early June, which is often referred to as "mass spawning," although the exact timing has not been fully understood with a range of a few weeks (e.g., Zayasu & Shinzato, 2016). Therefore, we designed the particle tracking model with the release timing at particular time in the evening for two weeks centered at the night proposed by Zayasu and Shinzato (2016). The 3-D particle tracking was thus conducted for every spring over the four model years from 2012 to 2015 to increase the statistical robustness and interannual variability. About 110,000 Lagrangian particles were equally distributed in the 224 patches and released every day for a two-week period in each of the four years. Hence, releases of particles take place 14 times each year, centered on the peak-spawning period that occurs at 8 P.M. local time on the day subsequent to the full moon (a spring tide) in May (Table 4). This release scenario mimics actual coral spawning with increased statistical significance by repeated releases.

4.2. Results

Figure 5 shows the connectivity matrix for the advection time of 21 days from the particle tracking experiment 1. The magnitude of the connectivity represents probability of particles transported from a source site to a sink site. Warmer (colder) colors correspond to higher (lower) connectivity of coral spawn and larvae between origins labeled in the abscissa and destinations in the ordinate. Evidently, high connectivity manifests on and around the straight line with a slope of 1:1 (viz., 45°) depicted by reddish colors, exhibiting that the particles mostly remain near the released areas even after the advection time of 21 days. Nevertheless, moderately high connectivity also appears in the lower right part of the matrix, relative to the straight line, than in the upper left part. This asymmetry demonstrates that the particles travel long distance to reach other islands, which we call "interisland remote connectivity" across the islands, with prevailing northeastward transport. Evidently, the northeastward drifting Kuroshio appears to play a key role in promoting

Table 3
Configurations for the Particle Tracking Experiments

	Experiment 1	Experiment 2
Number of patches	224	145
Diameter of patches	10 km	2 km
Release depth	3 m	3 m
Maximum advection time	21 days	21 days
Released particles/day (A)	110,000	280,000
Released time/year (B)	14 times	14 times
Total number of released particles ($A \times B$)	1,540,000	3,920,000

Table 4
Durations of Daily Particle Releases Mimicking Actual Coral Spawning

Year	Peak Spawning (Full Moon in May +1 day)	Release Durations (14 days)
2012	7 May	30 April–13 May
2013	26 May	19 May–1 June
2014	16 May	9–22 May
2015	5 May	28 April–11 May

such asymmetric transport. For instance, the connectivity for the long-distance transport from the southernmost area, including Ishigaki Island, Sekisei Lagoon, and Iriomote Island (which are collectively referred to as the Yaeyama Islands; sites #13–15 in Figure 1b), to Okinawa Island (#8; which is the largest island in the Nansei Archipelago, serving as the prefectural capital and the most popular tourist destination) are at O (10^{-3}). This result indicates that one single particle (i.e., coral spawn or larva) out of 1,000 released around the Yaeyama Islands may be transported northeastward more than 400 km to reach Okinawa Island within the advection time of 21 days. This numerical evaluation suggests that there is a significant interisland connectivity that is qualitatively consistent with the coral connectivity based on population genetics reported in Nakajima et al. (2010). Such interisland remote connectivity, most likely induced by the Kuroshio, would have considerable importance for determining marine protected areas suitable to maintain coral ecosystems. Therefore, we focused in the subsequent sections on the particles traveling long distances (hereinafter referred to as long-distance particles or LDPs) responsible for remote connectivity of coral spawn and larvae across the Nansei Archipelago.

5. Interisland Remote Connectivity

5.1. Particle Tracking Experiment 2

Another off-line Lagrangian particle tracking experiment (experiment 2; Table 3) was conducted to investigate LDPs responsible for the interisland remote connectivity. In experiment 2, we focused on LDPs originated from the Yaeyama Islands (the southernmost area in the Nansei Archipelago that includes the major islands of Ishigaki and Iriomote, with Sekisei Lagoon located between them; Figures 1c and 6a) as the source areas of coral spawn. In experiment 2, about 280,000 Lagrangian particles were released daily from 145 patches with a reduced diameter of 2 km defined around the Yaeyama Islands (Figure 6a). Hence, a total of ~3.9 million particles are analyzed. Other release procedures, the model configurations, and the rationale behind the experimental design are the same as those used in experiment 1 (sections 2.2 and 4.1). Before analyzing the interisland transport, the local connectivity matrix around the Yaeyama Islands averaged for the four-year model period is briefly discussed (Figure 6b). Similarly to the interisland connectivity matrix from experiment 1 (Figure 5), self-recruitment is predominant as illustrated by the highest connectivity around the 1:1 line. Sekisei Lagoon is a "hot spot" that intensively collects particles released from other sites, as represented by higher connectivity in the upper half of the matrix, particularly groups 14–18. There are several pinpoint connections such as 6➔1, 1➔5, 2➔16, and 10➔18, suggesting that local nearshore transport invokes anisotropic connections. Moreover, the southwestern coast of Ishigaki Island (groups 8–11) has less pronounced connectivity and does not receive many particles from remote sites within the Yaeyama Islands. Such intraisland connectivity is inevitable for management of the local marine protected areas, whereas we do not further discuss as it is beyond the scope of the present study.

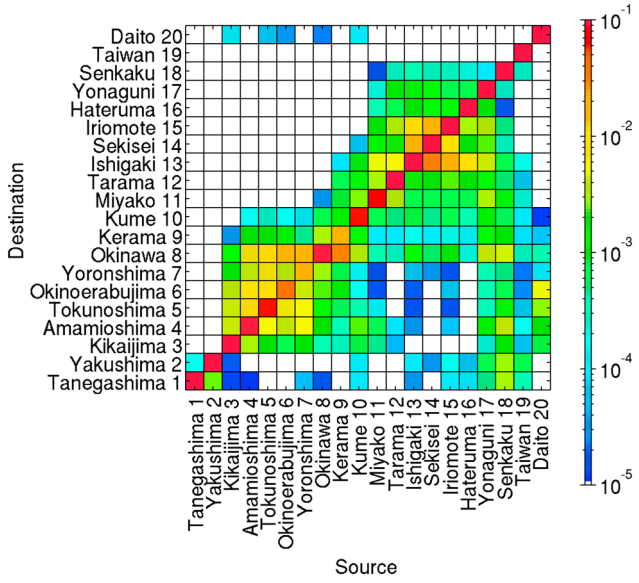

Figure 5. Connectivity matrix of coral spawn and larvae across the Nansei Archipelago for the advection time of 21 days from experiment 1. The numbers and names of the 19 islands and a lagoon shown in the abscissa and ordinate correspond to those presented in Figure 1b and Table 1.

For validation of the particle tracking model results, two sets of drifter data were utilized. The first one is composed of six surface drifters GPS-equipped released near Sekisei Lagoon during the spring tide in May and June, 2006 and 2007. The other set of drifter data is the publicly available one distributed as the Global Drifter Program (GDP) operated by NOAA (http://www.aoml.noaa.gov/phod/dac/index.php). This GDP data set consists of time series of the geographical positions of a large number of satellite-tracked surface drifting buoys. These buoys were mostly released in the deep ocean to minimize coastal influences. Therefore, it is suitable to use the GDP data for examining pelagic behaviors of particles.

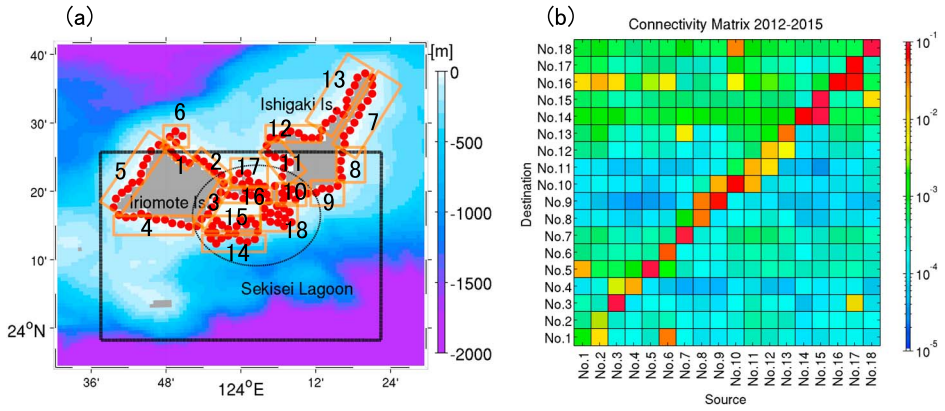

Figure 6. (a) Locations of the source patch sites for the particle tracking experiment 2 distributed around the Yaeyama Islands including Iriomote Islands, Ishigaki Islands, and Sekisei lagoon. Red circles indicate 145 patches with a diameter of 2 km, the dashed black rectangle is the domain for the spatial averaged velocity estimate in Figure 10, the dashed black oval approximates the area of Sekisei lagoon, and color shows bathymetry (m). The orange rectangles with numbers (1–18) represent the groups of source and destination patches used in (b). (b) The local connectivity matrix around the Yaeyama Islands from experiment 2 averaged over the four-year period from 2012 to 2015. The site group numbers in the abscissa and ordinate are as indicated in (a).

5.2. Advection Time-Averaged Lagrangian PDFs

Figure 7 presents trajectories of the six in situ surface drifters (section 5.1) on the modeled time-averaged Lagrangian PDFs, which are computed by taking averages of Lagrangian PDFs at 6-hr intervals over the advection time of 21 days for the four model years, from 2012 to 2015. Stated another way, the averaged Lagrangian PDFs are averages of 21 (days) × 4 (times a day) × 4 (model years) frames of the Lagrangian PDFs over the advection time of 21 days, representing relative magnitude of the probability of passage of the particles in *a climatological sense*. Therefore, interannual variability of the Lagrangian PDFs is significantly reduced allowing for qualitative comparisons to in situ drifter trajectories that did not synchronize with the model. It should be noted that the model years differ from the observation, mainly because a reliable high-resolution wind data set for the L2 model was not available (viz., the JMA GPV-Meso Scale Model; section 2.1) for 2006 and 2007. In Figure 7, warmer (colder) colors illustrate the regions with higher (lower) averaged PDFs, where the particles have passed more (less) frequently. The in situ surface drifter trajectories appear mostly in the regions where higher Lagrangian PDFs manifest, showing a good agreement with the model results *climatologically*. The observations reveal that only one single drifter was transported long distance in the north-eastward direction partly along the Kuroshio path (Figure 2a), whereas the other five drifters drifted around

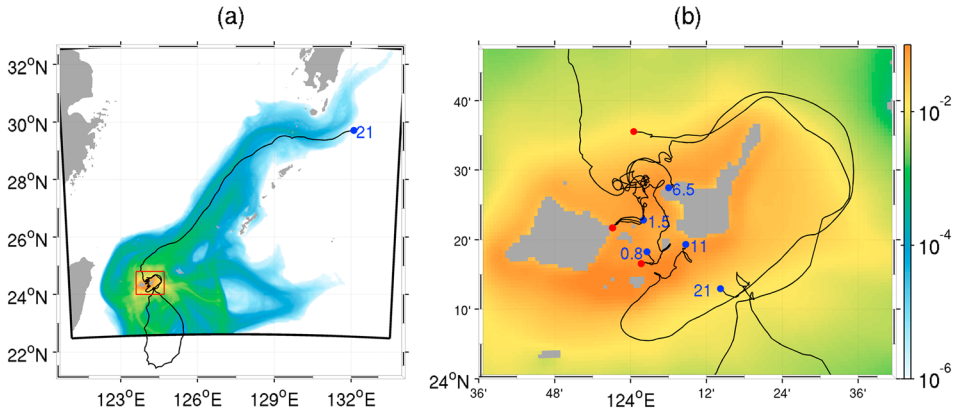

Figure 7. (a) Six in situ surface drifter's trajectories (black curves) on advection time-averaged Lagrangian PDF (color) over the advection time of 21 days for all the releases in 2012–2015. (b) Enlarged figure of (a) focusing on the Yaeyama Islands shown by the red box in (a). Red dots are the released positions of the drifters originated from Sekisei lagoon between Ishigaki and Iriomote Islands, while blue dots are the position of the drifters at the labeled advection times since drifters were released until they beached, or up to the maximum advection time of 21 days (unit: day).

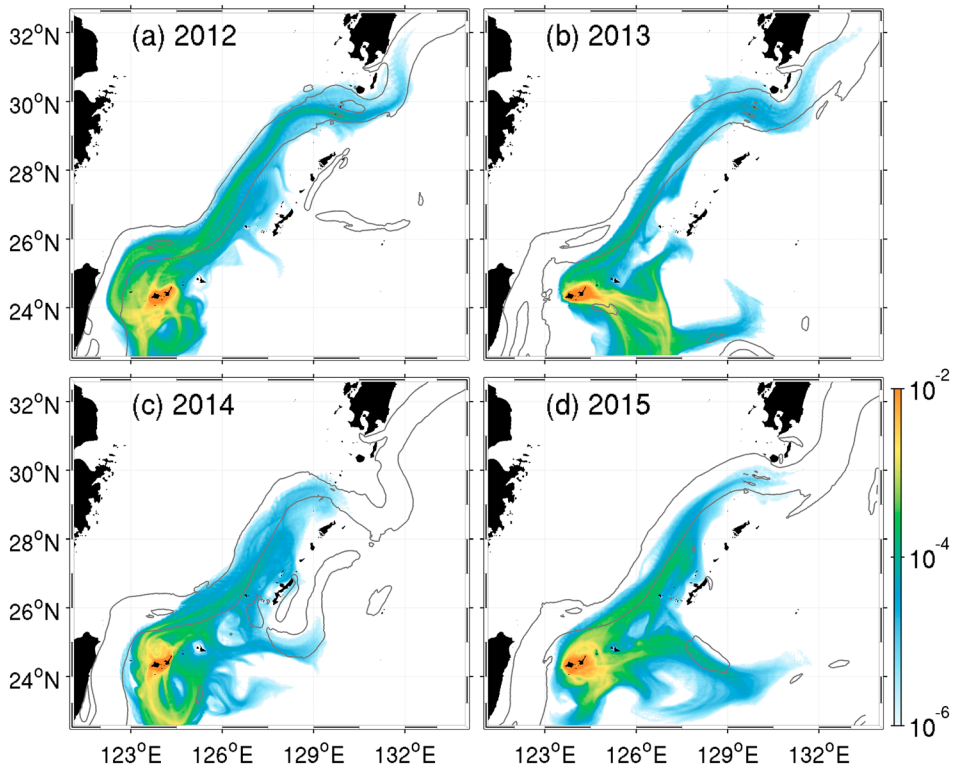

Figure 8. Averaged Lagrangian PDF for each of four years from 2012 to 2015. Thin black contours represent five-week averaged surface velocity magnitude of 0.5 m/s, showing approximate shapes of the Kuroshio path during the modeled coral spawn periods.

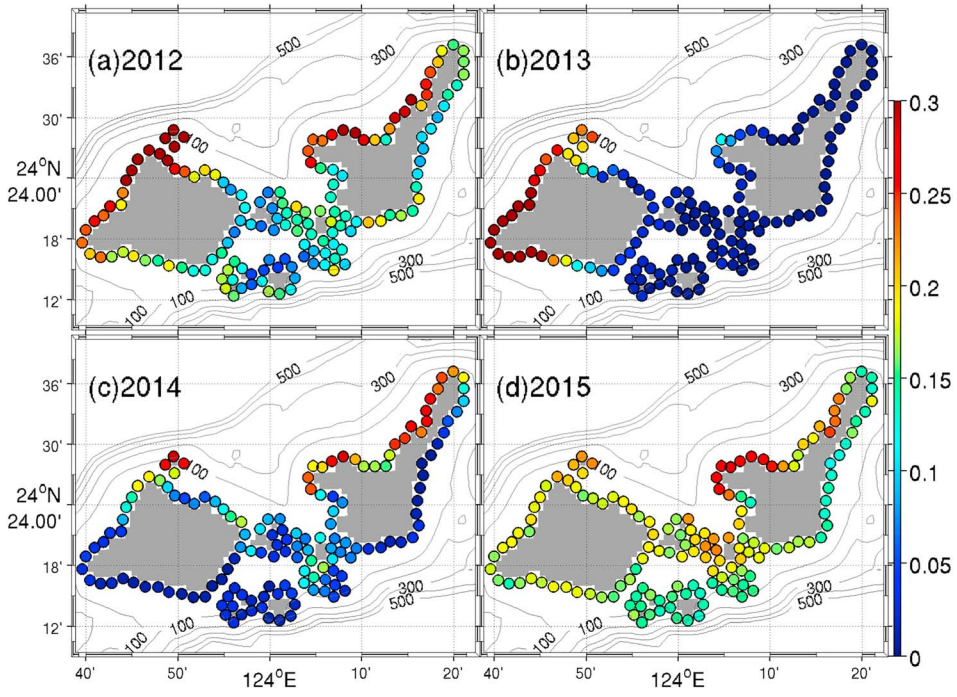

Figure 9. LDP (particles travel long distance to pass 26.5°N) probability at each release patch around the Yaeyama Islands. Contours are isobaths <500 m with intervals of 100 m.

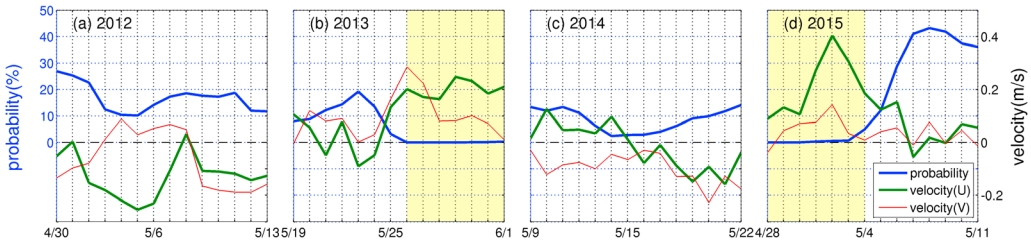

Figure 10. Time series of LDP probability averaged over all the 145 patches (blue) and eastward (green) and northward components of the modeled surface current velocity (red) for each of the particle release periods in 2012–2015. The velocities are spatially averaged over the dashed black rectangle in Figure 6.

the islands and beached within 21 days. These results are qualitatively consistent with the averaged PDF distribution, in which the highest PDFs appear near the release sites and the elongated, meridionally asymmetric far-field PDF pattern, as well as the connectivity matrix shown in Figure 5. Although coral spawn and larvae are largely constrained around Sekisei Lagoon (see also Figure 6b), a nontrivial population could travel long distance by entrained in the Kuroshio.

Subsequently, interannual variability of the averaged Lagrangian PDFs is investigated for each of the four model years (Figure 8). In all the four years, many of the particles travel northeastward as higher averaged PDFs manifested along the Kuroshio path depicted by thin black contours. However, there are obvious interannual differences in the spatial distributions of the averaged PDFs. For example, some particles reach 32°N and further north in 2012 and 2013, although almost no particle passes 30°N in 2014 and 2015. LDPs entrained in the Kuroshio travel northeastward, then are expelled to the east toward Okinawa Island (centered at 26°28′46″N and 127°55′40″E) most actively in 2014. Striking interannual variability in the PDFs is also found in the southeastern area of Sekisei Lagoon. In 2012 and 2014, many particles are dispelled southward, while in 2013 and 2015, high PDFs appear in the east of the lagoon. These results suggest the Kuroshio plays a central role in promoting the northeastward LDPs from the Yaeyama Islands, with pronounced interannual variability in the advection-time averaged Lagrangian PDFs, which could be associated with the transient Kuroshio path and other regional oceanic variability.

5.3. LDP Probability in the Yaeyama Islands

To investigate how the LDPs occur with significant interannual variability, the release sites around Sekisei Lagoon were revisited and the probability of LDP occurrence in each release patch for each year was

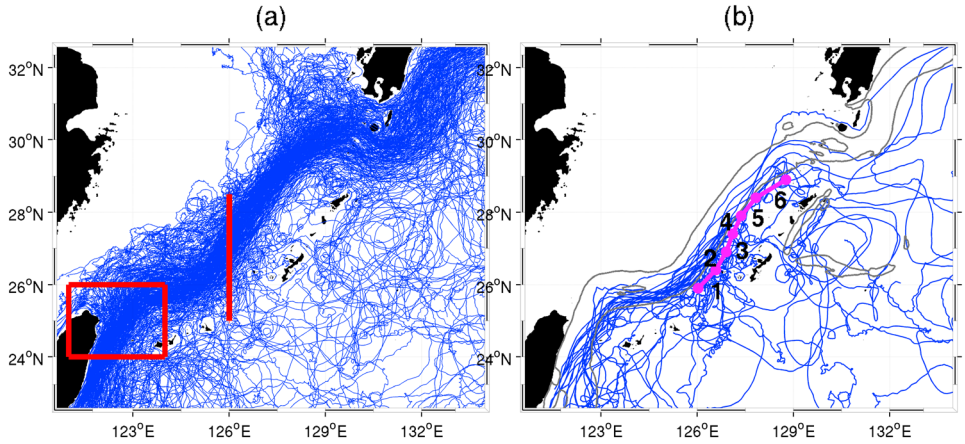

Figure 11. Selected trajectories of satellite-tracked surface drifters from the data set of the global drifter program. (a) The 296 trajectories of the extracted drifters entrained in the Kuroshio (blue curves), which have entered the red box (bounded by 121°E, 124°E, 24°N, and 26°N) once and then crossed the red line (at 126°E between 25°N and 28.5°N). (b) Trajectories of 24 drifters expelled from the Kuroshio (blue curves). Magenta lines: transects for extracting the drifters separated from the Kuroshio, corresponding approximately to the Kuroshio axis where the maximum velocity occurs. Black texts: the transect numbers (1–6) used in Figure 12. Gray contours: the five-week averaged surface velocity magnitude >0.5 m/s.

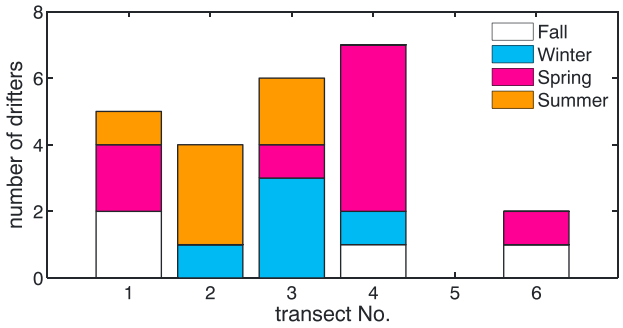

Figure 12. Number of the drifters crossing the six magenta transects (Figure 11b) and then drifting southward by the KCC. The horizontal axis represents the transect numbers shown in Figure 11b. Colors correspond to the seasons when the drifters crossed the magenta transects. The definition of the boreal seasons is as follows. Fall: October–December, winter: January–March, spring: April–June, and summer: July–September.

evaluated. In this case, the LDPs are defined as the particles passing 26.5°N due to intense advective effects of the Kuroshio. Figure 9 shows the probability of LDP around the Yaeyama Islands, in which the colors of patches correspond to the LDP probability. For instance, the LDP probability of 0.3 suggests that 30 particles out of 100 released from that patch travel long distance and pass 26.5°N to become LDPs. LDP probability is generally high in the northern coastal areas of the Yaeyama Islands, where released particles are readily entrained in the Kuroshio to travel long distance. In contrast, LDP probability near the southern coasts is much lower with larger interannual variability with quite low probability in 2013 and 2014. This result clearly indicates that the oceanic conditions south of Sekisei Lagoon could influence the number of LDPs.

We then examined possible causes for the interannual variability in LDP probability. Figure 10 shows time series of LDP probability and surface current velocities averaged over the black rectangle shown in Figure 6 for the 14-day release period in each year. The blue curves show the PDF probability averaged over all 145 patches around the Yaeyama Islands, and the green and red curves are the spatially averaged eastward and northward surface current velocities. The probability prominently changes as the release time changes, leading to the mean LDP variations in each year. Overall, the eastward velocity near the release sites and the LDP probability seem to have a correlation. The LDP probability is significantly suppressed with large eastward currents and moderate northward currents. This tendency is most evident during the latter half of 2013 and first half of 2015 in Figures 10b and 10d (yellow shades). Therefore, coral spawn released from the southern area of the lagoon is quite sensitive to eastward currents upon the release for becoming LDPs, even with mean northward currents.

6. Influences of the Kuroshio Counter Current (KCC)

6.1. Deviations From the Kuroshio: The Global Drifter Data Set

Relative positions between release sites and the Kuroshio, as well as local oceanic currents, are responsible for the transition to LDPs (section 5). The next question to be answered may be how are the LDPs that were once entrained in the Kuroshio extracted from the current to approach the islands? Before examining the model result, it is possible to make use of the satellite-tracked surface drifter data set from the GDP (section 5.1) to analyze the cross-Kuroshio (transverse), southeastward transport of the GDP drifters entrained once in the Kuroshio. Given the large number of the drifter trajectories observed from 1972 to 2017, the drifters that entered the red box once and then crossed the red transect were extracted (Figure 11a). This operation extracted a total of 269 drifters that were trapped and transported long distances by the Kuroshio in the study area. Blue curves in Figure 11a show their trajectories. A further selection was performed for the 269 drifters to extract the LDPs that crossed at least one of the six transects shown by the magenta lines in Figure 11b. The magenta transects depict connections between approximate locations of the Kuroshio axis, which were defined as the zonal positions where the maximum surface velocity occurs every 0.5° meridional bin between 26°N and 29°N in close proximity to the Kuroshio path. Sixty-three drifters out of 269 were found to have crossed the magenta lines from west to east, and 24 drifters drifted southward after crossing the magenta lines. This result quantifies that ~23% (i.e., 63/269) of the LDPs entrained in the Kuroshio are expelled and travel eastward, and ~9% (24/269) are subsequently transported southward.

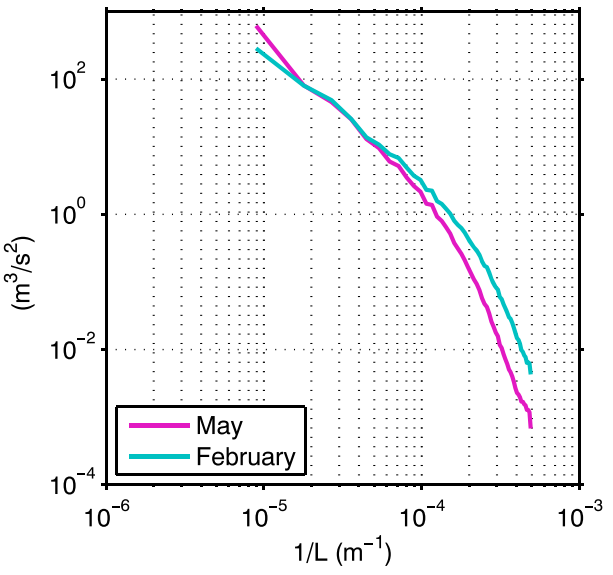

Figure 13. Surface kinetic energy wavenumber spectra for winter (February) and spring (May) in the magenta box in Figure 1a.

Figure 12 represents seasonal variability of the number of the drifters crossing the six magenta transects and then traveling southward. Twenty-two drifters out of 24 crossed southern transects 1–4 close to

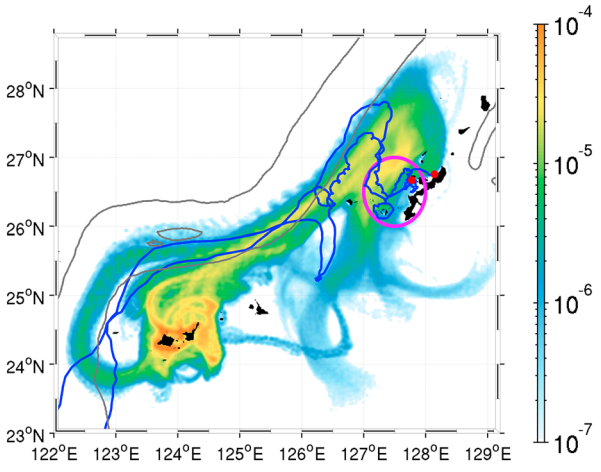

Figure 14. Averaged Lagrangian PDFs of the trapped LDPs over the advection time of 21 days from experiment 2 (color). Trajectories of two in situ drifters in the global drifter program data set that crossed transects 3 and 4 (Figure 11b) and then entered the magenta circle (blue curves) are depicted. Red dots are the final position of the two GDP drifters. Gray contours represent the five-week averaged surface velocity of 0.5 m/s.

Okinawa Island where the higher averaged Lagrangian PDFs extended westward from the Kuroshio path (Figure 8 and section 5.2). No drifter crossed transect 5, while the largest number of drifters crossed transect 4. Therefore, the separation of the LDPs from the Kuroshio and subsequent southward transport associated with the KCC opposed to the Kuroshio are crucial for promoting landward particle transport and thus interisland connectivity. Therefore, seasonal variability in Figure 12 depicts the period when more drifters are entrained in the KCC. The separation of the LDPs from the Kuroshio has frequently occurred in warmer seasons, most evidently in spring along transect 4.

A preliminary model experiment conducted in Uchiyama et al. (2016) suggested that the KCC developed between the Kuroshio and the Nansei Archipelago is accompanied by seasonally varying mesoscale eddies with diameters of O (100 km), which emerged most notably in spring. Figure 13 presents wavenumber kinetic energy spectra of surface currents from the ROMS-L2 model analyzed over the magenta box shown in Figure 1a for warm (boreal spring, May) and cold (boreal winter, February) seasons. The spectral slope in spring is steeper than in winter with significantly less energized kinetic energy for higher wavenumber components (i.e., submesoscale) with wavelengths $<O$ (10 km), while the lower wavenumber components (mesoscale) are decreased in winter. This result indicates that the KCC is likely accompanied by mesoscale eddies that develop in warmer seasons and propagate southwestward as Rossby waves. In turn, down-front, northerly seasonal wind and surface cooling in winter induce symmetric and baroclinic instability, leading to the emergence of submesoscale eddies (e.g., Kamidaira et al., 2018; Sasaki et al., 2014), which act to break up mesoscale eddies into smaller eddies. These results suggest

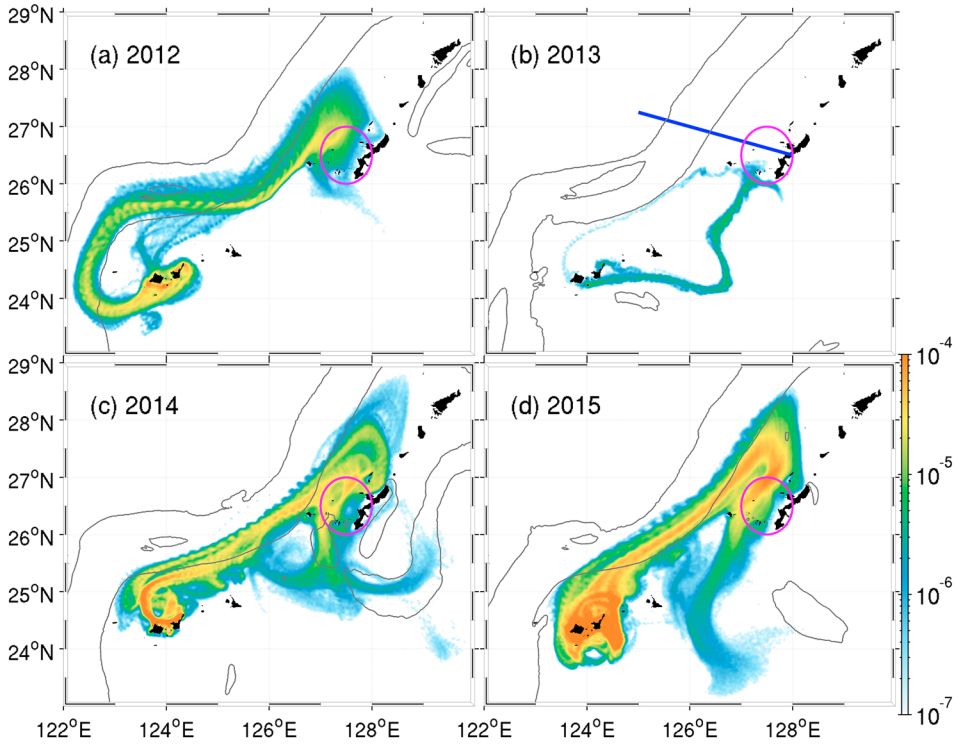

Figure 15. Averaged Lagrangian PDFs of the trapped LDPs (i.e., long-distance particles trapped by the KCC) for each year. Magenta circles: the domain for extracting the trapped LDPs as defined in Figure 14. The blue line in (b) is the transect for the KCC volume flux analysis in Table 5.

Table 5
Comparison Between the Time-Averaged Volume Transport of the KCC in Sverdrup (Sv; 10^6 m^3/s) and the Rate (%) of the Trapped LDPs Over the Total Number of Particles Released From the Lagoon, for Each of the Four Model Years

Year	2012	2013	2014	2015
Mean volume transport of the KCC (Sv)	3.94	6.24	7.02	17.21
Trapped LDPs/total particles × 100 (%)	0.70	0.03	1.31	2.89

Note. See the main text for detail.

that development of the KCC is more stable and persistent in spring, than other times of the year, when submesoscale activities in the upper ocean are lower. Evidently, this season corresponds to when coral spawning occurs. Less disturbed mesoscale eddies act to enhance lateral transverse mixing that promotes the eastward zonal transport of coral spawn and larvae expelled from the Kuroshio toward the west coast of the Nansei Archipelago.

6.2. LDPs Entrained by the KCC

Finally, we further examined the model result (experiment 2; Table 3) by extracting the LDPs entrained in the KCC near Okinawa Island that were responsible for interisland remote connectivity between the Yaeyama Islands and Okinawa Island. In doing this, we define the magenta circle as shown in Figure 14 and extracted the drifters released from the Yaeyama Islands that have entered the circle. Colors indicate the averaged Lagrangian PDFs of the LDPs trapped in the KCC (referred to as "trapped" LDPs) for the advection time of 21 days from experiment 2 (Table 3), while blue curves are the trajectories of two in situ GDP drifters crossing the circle and drifted toward the west coast of Okinawa Island. The separation of the two in situ drifters from the Kuroshio has occurred on 13 July 2011 and 26 June 2013, viz., in warmer seasons. The distribution of the averaged Lagrangian PDFs of the trapped LDPs (colors) and the trajectories of the two in situ drifters (blue curves) are closely correlated each other, reassuring that the model does a moderately good job in a climatological sense. The trajectories of the two drifters abruptly separated from the Kuroshio were entrained in the KCC and drifted southeastward, similarly to the modeled PDFs.

Figure 15 shows averaged Lagrangian PDFs of the trapped LDPs for each of the four model years. Table 5 summarizes the rate (in %) of the trapped LDPs relative to the total number of the released particles, and the time-averaged southwestward volume transport (in Sv) of the KCC across the transect shown by the blue line in Figure 15b. The period for the time-averaging operation is 35 days including 14 days of the particles releasing period plus the advection time of 21 days, and thus for the entire spawning period in spring. Overall, the rate of the trapped LDPs is linearly correlated with the KCC volume transport, except for 2013. In spring of 2013, the LDPs were much less as shown in Figure 15b because of the considerably reduced LDPs associated with the eastward currents near the release site (section 5.3). The KCC transport is largest in 2015 with the increase of the trapped LDPs of ~3%. This rate is nontrivial because 3% means that three coral individuals out of 100 born in the lagoon travel more than 400 km to reach Okinawa Island anisotropically only within 21 days. The KCC intensity largely contributes to enhancement of the zonal particle transport from the Kuroshio to Okinawa Island, and thus, to increase of the interisland remote connectivity.

7. Discussion and Conclusions

Toward optimal preservation and restoration of the coral habitats around the Nansei Archipelago, the ECS, we quantified the coastal connectivity of corals across the islands using a double-nested high-resolution synoptic ocean model based on ROMS, coupled with a 3-D off-line Lagrangian particle tracking model. Our central scientific question posed was how interisland, remote connectivity is provoked. We successfully demonstrated that long-distance larval transport and resultant interisland connectivity were primarily induced by the Kuroshio that persistently drifts northeastward on the continental shelf break of the ECS near the study area.

The connectivity matrix of 19 major islands and one lagoon over the archipelago indicated that most of the particles (corals) remain near the released area. However, a modest amount of the particles drifts primarily northeastward, in the direction of the Kuroshio, and finally reaches other islands in the advection time of 21 days. The interisland connectivity is apparent even for pairs of islands ~1,000 km apart from each other, with tolerable southwestward connections as well. These primary findings are consistent with previous genetic population studies. For instance, Nakajima et al. (2010) examined the population genetics of *A. digitifera* using highly variable markers at 19 sites in seven regions along the Nansei Archipelago. They confirmed the existence of high genetic connectivity with significant genetic differentiation among populations in geographically close sites and regions, without losing genetic diversity, leading to complex and various connective patterns. Such disagreement between genetic connectivity and geographic distance in the *A. digitifera*

populations were also reported in Nishikawa and Sakai (2005) within the southern Nansei Archipelago. Shinzato et al. (2015) concluded from the decoded genome of *A. digitifera* that the population structure in the southern Nansei Archipelago is influenced by infrequent long-distance dispersal over the SRA. They detected strong historical migration from the Yaeyama Islands (YIs) to Okinawa Island. Zayasu et al. (2016) reported from 13 microsatellite markers of *A. tenuis* sampled at 15 location across the Nansei Archipelago that genetic population structure is complex as gene flow not only occurs from south to north but also from north to south in various locations. Hence, the YIs and the Amami Islands (the islands #3–7 in Table 1) are potential northern and southern sources of corals, while Miyako Island (#11) and west central Okinawa Island are potential sink populations.

The present numerical study provides the mechanism responsible for maintaining the interisland connectivity with experiment 2, where corals were released from the YIs. The larval dispersal was asymmetrically elongated in the direction of the Kuroshio and is consistent with the trajectories of the in situ surface drifters. One deployed in situ drifter out of six was entrained in the Kuroshio and traveled a considerably long distance northeast for ~1,000 km in 21 days, as solid evidence of a key role played by the Kuroshio. Although the corals released from the northern coasts of the YIs were readily entrained in and transported long distances by the Kuroshio, those from the southern coasts resulted in notably suppressed entrainment due to the prevailing eastward currents invoked upon the releases. With a guide of the satellite-tracked global surface drifter data set, the model confirmed separation of particles from the Kuroshio and subsequent eastward transport to the western shore of Okinawa Island, occurring particularly in warmer seasons. A key influencer of eastward zonal transport is the Kuroshio Counter Current (KCC), which is formed between the Kuroshio and the Nansei Archipelago and drifts southwestward. The larger volume the KCC has to transport, the more intensive separation from the Kuroshio occurs.

Previous numerical connectivity studies for other areas with abundant corals, such as the Great Barrier Reef (GBR), Australia, generally have concluded that local larval transport is relatively important and primarily unrelated to ambient currents. For the GBR and other coastal sites around Australia, recent numerical connectivity studies (e.g., Hock et al., 2014; Kool & Nichol, 2015; Wood et al., 2014) mainly have focused on sensitivity to individual behavior models (e.g., diel vertical migration), while dynamical roles in population connections have been poorly explored. This is partly because, for settlement of larvae responsible for coral connectivity along GBR, neashore retention, or so-called "stickiness," is believed to be most crucial in trapping larvae as compared to dynamical effects from offshore currents (e.g., Wolanski et al., 1989; Wolanski and Kingston, 2014). However, a satellite observation suggested a possible implication of topographically generated mesoscale eddy associated with the southward drifting East Australia Current for ecological linkage in the southern GBR (Weeks et al., 2010). By contrast, Garavelli et al. (2016) analyzed larval dispersal along the Chilean coasts based on a climatological ROMS model output at 4-km lateral resolution. They demonstrated that advective dynamics predominantly controls the major separation feature of the coastal population connection, which always occurred at around 29–30°S, regardless of choices of behavior models. Another ecologically important coral habitat, the Florida Keys in the Straits of Florida, USA, was reported to be influenced both by two branches of the Gulf Stream, that is, the Loop Current in the Gulf of Mexico and the eastward drifting Florida Current in the Florida Straits, based on a multinested high-resolution HYCOM model (Kourafalou et al., 2018; Sponaugle et al., 2012). Dominant transport occurred eastward along the Florida Current, whereas a weak upstream (westward) transport was also observed (Paris et al., 2013). These studies have anticipated that the balance between these two major currents alters the Southwestern Florida Shelf circulation and associated mesoscale eddies, leading to substantial impacts on the regional coral connectivity.

The present study in the Nansei Archipelago and the previous studies in other areas have suggested that the intensive advective transport due to persistent and/or transient oceanic currents and associated eddies could be crucial factors that control the remote population connectivity. However, detachment from and settlement in the nearshore areas are another yet to be fully understood processes in literature. We evidently presented insights into such processes affected not only by the Kuroshio but also by local dynamics accounting for the entrainment rate of pelagic particles in the Kuroshio upon the release, secondary processes such as those by the KCC responsible for transverse expelling transport from the Kuroshio to islands, and seasonally varying submesoscale dynamics. As have pointed out by Werner et al. (2007), Siegel et al. (2008), and White et al. (2010), we emphasize here that numerical connectivity studies require high-resolution models,

preferably down to submesoscale eddy-resolving resolutions with grid spacing of ~1 km (e.g., Kamidaira et al., 2018), to properly account for advective effects to minimize uncertainty of overly simplified diffusive transport assumption in genetic approaches.

Furthermore, it is worth noting that effects from surface gravity waves are omitted in the present model, even though waves are anticipated to substantially influence regional and local circulations and the associated coral transport through Stokes advection, the Stokes-Coriolis force, and wave setup and littoral currents induced by breaking waves (e.g., Uchiyama et al., 2010). These factors respectively contribute to altering Lagrangian particle transport through additional Stokes drift velocity, modifying the geostrophic and Ekman balances particularly in the upper oceans, and changing nearshore hydrodynamics and resultant particle transport near reefal edges through sporadic offshore eruption by transient rip currents and/or energetic alongshelf transport by wave-driven longshore currents (e.g., Uchiyama et al., 2009; Uchiyama, Kanki, et al., 2017; Weir et al., 2011). As a consequence, it is hypothesized that the coral transport and resultant connectivity may be altered by (1) additional wave-induced residual coral transport developed in the direction of wave and swell propagation and (2) more pronounced cross-shore exchange and alongshore transport in the nearshore shallow areas. The former may introduce large-scale biases in the coral transport pattern, while the latter may enhance the coral recruitment in the spawning and potential settlement sites around reefal edges, which are germane to maintaining abundant coral community. A quantitative assessment of these factors is beyond the scope of the present study, but they must be taken into account in future works, in particular when models will have much higher resolutions at *O* (10 m) to sufficiently resolve the surf zone.

Acknowledgments

This research was financially supported by the Japan Society for the Promotion of Science (JSPS) Grant-in-aid for Scientific Research (grants 15H04049, 15KK0207, and 18H03798 at Kobe University and 17K00653 at Kobe Gakuin University). The supplementary files contain simulation data that enable the figures to be reproduced. The model output and computing codes used in this study are available from the authors upon request (uchiyama@harbor.kobe-u.ac.jp). The JCOPE2 reanalysis data set is freely available for scientific purposes upon request to APL/JAMSTEC (jcope@jamstec.go.jp). The STRM30_Plus data are available at ftp://topex.ucsd.edu/pub/srtm30_plus/. The J-EGG500 data set is distributed by the JODC at http://jdoss1.jodc.go.jp/cgi-bin/1997/depth500_file. The mapped sea level anomaly in delayed-time product was generated by Ssalto/Duacs and distributed by AVISO (ftp.aviso.altimetry.fr). The GPV-GSM/MSM atmospheric product was generated by the JMA, and it is available from the repository at http://database.rish.kyoto-u.ac.jp/arch/jmadata/data/gpv/original/. The COADS data are maintained and distributed by NOAA at https://www.esrl.noaa.gov/psd/data/gridded/data.coads.1deg. The Global Drifter Program data set is processed and distributed at http://www.aoml.noaa.gov/phod/dac/index.php by NOAA/AOML.

References

Andres, M., Park, J. H., Wimbush, M., Zhu, X. H., Chang, K. I., & Ichikawa, H. (2008). Study of the Kuroshio/Ryukyu current system based on satellite-altimeter and in situ measurements. *Journal of Oceanography*, *64*(6), 937–950. https://doi.org/10.1007/s10872-008-0077-2

Becker, J. J., Sandwell, D. T., Smith, W. H. F., Braud, J., Binder, B., Depner, J., et al. (2009). Global bathymetry and elevation data at 30 arc seconds resolution: SRTM30_PLUS. *Marine Geodesy*, *32*(4), 355–371. https://doi.org/10.1080/01490410903297766

Bellwood, D. R., Hughes, T. P., Folke, C., & Nyström, M. (2004). Confronting the coral reef crisis. *Nature*, *429*(6994), 827–833. https://doi.org/10.1038/nature02691

Bentamy, A., Ayina, L. H., Queffeulou, P., Croize-Fillon, D., & Kerbaol, V. (2007). Improved near real time surface wind resolution over the Mediterranean Sea. *Ocean Science*, *3*(2), 259–271. https://doi.org/10.5194/os-3-259-2007

Carr, S. D., Capet, X., McWillimas, J. C., Pennington, J. T., & Chazez, F. P. (2008). The influence of diel vertical migration on zooplankton transport and recruitment in an upwelling region: Estimates from a coupled behavioral-physical model. *Fisheries Oceanography*. https://doi.org/10.1111/j.1365-2419.2007.00447.x

Chalker, B. E., Barnes, D. J., Dunlap, W. C., & Jokiel, P. L. (1988). Light and reef-building corals. *Interdisciplinary Science Reviews*, *13*(3), 222–237. https://doi.org/10.1179/isr.1988.13.3.222

Chassignet, E. P., Hurlburt, H. E., Smedstad, O. M., Halliwell, G. R., Hogan, P. J., Wallcraft, A. J., et al. (2007). The HYCOM (HYbrid Coordinate Ocean model) data assimilative system. *Journal of Marine Systems*, *65*(1-4), 60–83. https://doi.org/10.1016/j.jmarsys.2005.09.016

Connell, J. H. (1978). Diversity in tropical rain forests and coral reefs. *Science*, *199*(4335), 1302–1310. https://doi.org/10.1126/science.199.4335.1302

Dai, A., Qian, T., Trenberth, K. E., & Milliman, J. D. (2009). Changes in continental freshwater discharge from 1948 to 2004. *Journal of Climate*, *22*(10), 2773–2792. https://doi.org/10.1175/2008JCLI2592.1

Egbert, G. D., Bennett, A. F., & Foreman, M. G. (1994). TOPEX/POSEIDON tides estimated using a global inverse model. *Journal of Geophysical Research*, *99*, 24,821–24,852. https://doi.org/10.1029/94JC01894

Egbert, G. D., & Erofeeva, S. Y. (2002). Efficient inverse modeling of barotropic ocean tides. *Journal of Atmospheric and Oceanic Technology*, *19*(2), 183–204. https://doi.org/10.1175/1520-0426(2002)019<0183:EIMOBO>2.0.CO;2

Garavelli, L., Colas, F., Verley, P., Kaplan, D. M., Yannicelli, B., & Lett, C. (2016). Influence of biological factors on connectivity patterns for *Concholepas concholepas* (loco) in Chile. *PLoS One*, *11*(1), e0146418. https://doi.org/10.1371/journal.pone.0146418

Hayward, D. C., Hetherington, S., Behm, C. A., Grasso, L. C., Forêt, S., Miller, D. J., & Bell, E. E. (2011). Differential gene expression at coral settlement and metamorphosis—A subtractive hybridization study. *PLoS One*, *6*(10), e26411. https://doi.org/10.1371/journal.pone.0026411

Hisaki, Y., & Imadu, C. (2009). Southward recirculation of the East China Sea Kuroshio west of Okinawa Island. *Journal of Geophysical Research*, *114*, C06013. https://doi.org/10.1029/2008JC004943

Hock, K., Wolff, N. H., Condie, S. A., Anthony, K. R. N., & Mumby, P. J. (2014). Connectivity networks reveal the risks of crown-of-thorns starfish outbreaks on the great barrier reef. *Journal of Applied Ecology*, *51*(5), 1188–1196. https://doi.org/10.1111/1365-2664.12320

Hoegh-Guldberg, O. (1999). Climate change, coral bleaching and the future of the world's coral reefs. *Marine and Freshwater Research*, *50*(8), 839–866. https://doi.org/10.1071/MF99078

Hoegh-Guldberg, O., & Smith, G. J. (1989). The effect of sudden changes in temperature, light and salinity on the population density and export of zooxanthellae from the reef corals *Stylophora pistillata* Esper and *Seriatopora hystrix* Dana. *Journal of Experimental Marine Biology and Ecology*, *129*(3), 279–303. https://doi.org/10.1016/0022-0981(89)90109-3

Ichikawa, H., & Beardsley, R. C. (1993). Temporal and spatial variability of volume transport of the Kuroshio in the East China Sea. *Deep Sea Research Part I*, *40*(3), 583–605. https://doi.org/10.1016/0967-0637(93)90147-U

Ichikawa, H., & Beardsley, R. C. (2002). The current system in the Yellow and East China Seas. *Journal of Oceanography*, *58*(1), 77–92. https://doi.org/10.1023/A:1015876701363

Ichikawa, H., & Chaen, M. (2000). Seasonal variation of heat and freshwater transports by the Kuroshio in the East China Sea. *Journal of Marine Systems*, *24*(1-2), 119–129. https://doi.org/10.1016/S0924-7963(99)00082-2

Ichikawa, H., Nakamura, H., Nishina, A., & Higashi, M. (2004). Variability of northeastward current southeast of northern Ryukyu Islands. *Journal of Oceanography*, *60*(2), 351–363. https://doi.org/10.1023/B:JOCE.0000038341.27622.73

Ikeda, E., Iryu, Y., Sugihara, K., Ohba, H., & Yamada, T. (2006). Bathymetry, biota and sediments on the Hirota reef, Tane-ga-Shima—The northernmost coral reef in the Ryukyu Islands. *Island Arc*, *15*(4), 407–419. https://doi.org/10.1111/j.1440-1738.2006.00538.x

Johns, W. E., Lee, T. N., Zhang, D., Zantopp, R., Liu, C. T., & Yang, Y. (2001). The Kuroshio east of Taiwan: Moored transport observations from the WOCE PCM-1 array. *Journal of Physical Oceanography*, *31*(4), 1031–1053. https://doi.org/10.1175/1520-0485(2001)031<1031:TKEOTM>2.0.CO;2

Kamidaira, Y., Uchiyama, Y., Kawamura, H., Kobayashi, T., & Furuno, A. (2018). Submesoscale mixing on initial dilution of the radionuclides released from the Fukushima Dai-ichi nuclear power plant. *Journal of Geophysical Research: Oceans*, *123*, 2808–2828. https://doi.org/10.1002/2017JC013359

Kamidaira, Y., Uchiyama, Y., & Mitarai, S. (2017). Eddy-induced transport of the Kuroshio warm water around the Ryukyu Islands in the East China Sea. *Continental Shelf Research*, *143*, 206–218. https://doi.org/10.1016/j.csr.2016.07.004

Kool, J. T., & Nichol, S. L. (2015). Four-dimensional connectivity modelling with application to Australia's north and northwest marine environments. *Environmental Modelling and Software*, *65*, 67–78. https://doi.org/10.1016/j.envsoft.2014.11.022

Kourafalou, V. H., Androulidakis, Y. S., Kang, H., Smith, R. H., & Valle-Levinson, A. (2018). Physical connectivity between pulley ridge and Dry Tortugas coral reefs under the influence of the loop current/Florida current system. *Progress in Oceanography*, *165*, 75–99. https://doi.org/10.1016/j.pocean.2018.05.004

Le Traon, P. Y., Nadal, F., & Ducet, N. (1998). An improved mapping method of multisatellite altimeter data. *Journal of Atmospheric and Oceanic Technology*, *15*(2), 522–534. https://doi.org/10.1175/1520-0426(1998)015<0522:AIMMOM>2.0.CO;2

Liu, Y., Dong, C., Guan, Y., & Nencioli, F. (2012). Eddy analysis in the subtropical zonal band of the North Pacific Ocean. *Deep Sea Research Part I: Oceanographic Research Papers*, *68*, 54–67. https://doi.org/10.1016/j.dsr.2012.06.001

Mason, E., Molemaker, J., Shchepetkin, A. F., Colas, F., McWilliams, J. C., & Sangrà, P. (2010). Procedures for offline grid nesting in regional ocean models. *Ocean Modelling*, *35*(1), 1–15.

Mitarai, S., Siegel, D. A., Watson, J. R., Dong, C., & McWilliams, J. C. (2009). Quantifying connectivity in the coastal ocean with application to the Southern California Bight. *Journal of Geophysical Research*, *114*, C10026. https://doi.org/10.1029/2008JC005166

Miyazawa, Y., Zhang, R., Guo, X., Tamura, H., Ambe, D., Lee, J., et al. (2009). Water mass variability in the western North Pacific detected in 15-year eddy resolving ocean reanalysis. *Journal of Oceanography*, *65*(6), 737–756. https://doi.org/10.1007/s10872-009-0063-3

Moberg, F., & Folke, C. (1999). Ecological goods and services of coral reef ecosystems. *Ecological Economics*, *29*(2), 215–233. https://doi.org/10.1016/S0921-8009(99)00009-9

Munday, P. L., Leis, J. M., Lough, J. M., Paris, C. B., Kingsford, M. J., Berumen, M. L., & Lambrechts, J. (2009). Climate change and coral reef connectivity. *Coral Reefs*, *28*(2), 379–395. https://doi.org/10.1007/s00338-008-0461-9

Nakajima, Y., Nishikawa, A., Iguchi, A., & Sakai, K. (2010). Gene flow and genetic diversity of a broadcast-spawning coral in northern peripheral populations. *PLoS One*, *5*(6), e11149. https://doi.org/10.1371/journal.pone.0011149

Nakamura, M., Murakami, T., Khono, H., Noda, W., Matsushita, Y., & Mizutani, A. (2017). Coral recruitment on a local scale in Amitori Bay, Iriomote Island, estimated by settlement plates and numerical analysis. *Journal of Japan Society of Civil Engineers Series B2*, *73*(2), 1279–1284. https://doi.org/10.2208/kaigan.73.I_1279 (in Japanese with English abstract)

Nishikawa, A., Katoh, M., & Sakai, K. (2003). Larval settlement rates and gene flow of broadcast-spawning (*Acropora tenuis*) and planula-brooding (*Stylophora pistillata*) corals. *Marine Ecology Progress Series*, *256*, 87–97. https://doi.org/10.3354/meps256087

Nishikawa, A., & Sakai, K. (2005). Settlement-competency period of planulae and genetic differentiation of the scleractinian coral *Acropora digitifera*. *Zoological Science*, *22*(4), 391–399. https://doi.org/10.2108/zsj.22.391

Nozawa, Y., & Okubo, N. (2011). Survival dynamics of reef coral larvae with special consideration of larval size and the genus Acropora. *The Biological Bulletin*, *220*(1), 15–22. https://doi.org/10.1086/BBLv220n1p15

Paris, C. B., Helgers, J., Van Sebille, E., & Srinivasan, A. (2013). Connectivity modeling system: A probabilistic modeling tool for the multi-scale tracking of biotic and abiotic variability in the ocean. *Environmental Modelling and Software*, *42*, 47–54. https://doi.org/10.1016/j.envsoft.2012.12.006

Paulay, G. (1997). Diversity and distribution of reef organisms. In *Life and Death of Coral Reefs* (pp. 298–353). New York: Chapman & Hall.

Qin, D., Wang, J., Liu, Y., & Dong, C. (2015). Eddy analysis in the eastern China Sea using altimetry data. *Frontiers of Earth Science*, *9*(4), 709–721. https://doi.org/10.1007/s11707-015-0542-3

Qiu, B., & Imasato, N. (1990). A numerical study on the formation of the Kuroshio counter current and the Kuroshio branch current in the East China Sea. *Continental Shelf Research*, *10*(2), 165–184. https://doi.org/10.1016/0278-4343(90)90028-K

Rodríguez, E., Morris, C. S., Belz, J. E., Chapin, E. C., Martin, J. M., Daffer, W., & Hensley, S. (2005). *An assessment of the SRTM topographic products* (143 p.). Technical Report JPL D-31639, Jet Propulsion Laboratory, Pasadena, California.

Romero, L., Uchiyama, Y., Ohlmann, C., McWilliams, J. C., & Siegel, D. A. (2013). Particle-pair dispersion in the Southern California coastal zone. *Journal of Physical Oceanography*, *43*(9), 1862–1879. https://doi.org/10.1175/JPO-D-13-011.1

Sasaki, H., Klein, P., Qiu, B., & Sasai, Y. (2014). Impact of oceanic-scale interactions on the seasonal modulation of ocean dynamics by the atmosphere. *Nature Communications*, *5*(1), 5636. https://doi.org/10.1038/ncomms6636

Shchepetkin, A. F., & McWilliams, J. C. (2005). The Regional Ocean Modeling System (ROMS): A split-explicit, free-surface, topography-following-coordinate oceanic model. *Ocean Modelling*, *9*(4), 347–404. https://doi.org/10.1016/j.ocemod.2004.08.002

Shchepetkin, A. F., & McWilliams, J. C. (2008). Computational kernel algorithms for fine-scale, multiprocess, longtime oceanic simulations. In R. Temam, & J. Tribbia (Eds.), *Handbook of Numerical Analysis*, (pp. 119–181). Amsterdam: Elsevier. https://doi.org/10.1016/S1570-8659(08)01202-0

Shimokawa, S., Murakami, T., Ukai, A., Kohno, H., Mizutani, A., & Nakase, K. (2014). Relationship between coral distributions and physical variables in Amitori Bay, Iriomote Island, Japan. *Journal of Geophysical Research: Oceans*, *119*, 8336–8356. https://doi.org/10.1002/2014JC010307

Shinzato, C., Mungpakdee, S., Arakaki, N., & Satoh, N. (2015). Genome-wide SNP analysis explains coral diversity and recovery in the Ryukyu archipelago. *Scientific Reports*, *5*(1), 18211. https://doi.org/10.1038/srep18211

Siegel, D. A., Mitarai, S., Costello, C. J., Gaines, S. D., Kendall, B. E., Warner, R. R., & Winters, K. B. (2008). The stochastic nature of larval connectivity among nearshore marine populations. *Proceedings of the National Academy of Sciences of the United States of America*, *105*(26), 8974–8979. https://doi.org/10.1073/pnas.0802544105

Sponaugle, S., Paris, C., Walter, K. D., Kourafalou, V., & D'Alessandro, E. (2012). Observed and modeled larval settlement of a reef fish to the Florida keys. *Marine Ecology Progress Series*, *453*, 201–212. https://doi.org/10.3354/meps09641

Tada, H., Uchiyama, Y., & Masunaga, E. (2018). Impacts of two super typhoons on the Kuroshio and marginal seas on the Pacific coast of Japan. *Deep-Sea Research Part I*, *132*, 80–93. https://doi.org/10.1016/j.dsr.2017.12.007

Tamura, H., Nadaoka, K., & Paringit, E. C. (2007). Hydrodynamic characteristics of a fringing coral reef on the east coast of Ishigaki Island, Southwest Japan. *Coral Reefs*, *26*(1), 17–34. https://doi.org/10.1007/s00338-006-0164-z

Uchiyama, Y., Idica, E., McWilliams, J. C., & Stolzenbach, K. D. (2014). Wastewater effluent dispersal in Southern California bays. *Continental Shelf Research*, *76*, 36–52. https://doi.org/10.1016/j.csr.2014.01.002

Uchiyama, Y., Kanki, R., Takano, A., Yamazaki, H., & Miyazawa, Y. (2017). Mesoscale reproducibility in regional ocean modeling with a 3-D stratification estimate based on Aviso-Argo data. *Atmosphere-Ocean*, *56*(4), 212–229. https://doi.org/10.1080/07055900.2017.1399858

Uchiyama, Y., McWilliams, J. C., & Akan, C. (2017). Three-dimensional transient rip currents: Bathymetric excitation of low-frequency intrinsic variability. *Journal of Geophysical Research: Oceans*, *122*, 5826–5849. https://doi.org/10.1002/2017JC013005

Uchiyama, Y., McWilliams, J. C., & Restrepo, J. M. (2009). Wave-current interaction in nearshore shear instability analyzed with a vortex-force formalism. *Journal of Geophysical Research*, *114*, C06021. https://doi.org/10.1029/2008JC005135

Uchiyama, Y., McWilliams, J. C., & Shchepetkin, A. F. (2010). Wave-current interaction in an oceanic circulation model with a vortex force formalism: Application to the surf zone. *Ocean Modelling*, *34*(1–2), 16–35. https://doi.org/10.1016/j.ocemod.2010.04.002

Uchiyama, Y., Odani, S., Yamanishi, T., Kamidaira, Y., & Mitarai, S. (2016). Impact of mesoscale recirculation of the Kuroshio on asymmetric oceanic structure around Okinawa Island. *Journal of Japan Society of Civil Engineers Series B2*, *72*(2), I_481–I_486. https://doi.org/10.2208/kaigan.72.I_481 (in Japanese with English abstract)

Uchiyama, Y., Suzue, Y., & Yamazaki, H. (2017). Eddy-driven nutrient transport and associated upper-ocean primary production along the Kuroshio. *Journal of Geophysical Research: Oceans*, *122*, 5046–5062. https://doi.org/10.1002/2017JC012847

Uchiyama, Y., Zhang, X., Suzue, Y., Kosako, T., Miyazawa, Y., & Nakayama, A. (2018). Residual effects of treated effluent diversion on a seaweed farm in a tidal strait using a multi-nested high-resolution 3-D circulation-dispersal model. *Marine Pollution Bulletin*, *130*, 40–54. https://doi.org/10.1016/j.marpolbul.2018.03.007

Veron, J. E. N. (1986). *Corals of Australia and the Indo-Pacific*. North Ryde, NSW, Australia: Angus & Robertson.

Weeks, S. J., Bakun, A., Steinberg, C. R., Brinkman, R., & Hoegh-Guldberg, O. (2010). The Capricorn Eddy: A prominent driver of the ecology and future of the southern great barrier reef. *Coral Reefs*, *29*(4), 975–985. https://doi.org/10.1007/s00338-010-0644-z

Weir, B., Uchiyama, Y., Lane, E. M., Restrepo, J. M., & McWilliams, J. C. (2011). A vortex-force analysis of the interaction of rip currents and gravity waves. *Journal of Geophysical Research*, *116*, C05001. https://doi.org/10.1029/2010JC006232

Werner, F. E., Cowen, R. K., & Paris, C. B. (2007). Coupled biological and physical models: Present capabilities and necessary developments for future studies of population connectivity. *Oceanography*, *20*(3), 54–69. https://doi.org/10.5670/oceanog.2007.29

White, C., Selkoe, K. A., Watson, J., Siegel, D. A., Zacherl, D. C., & Toonen, R. J. (2010). Ocean currents help explain population genetic structure. *Proceedings of the Royal Society B*, *277*(1688), 1685–1694. https://doi.org/10.1098/rspb.2009.2214

Wolanski, E., Burrage, D., & King, B. (1989). Trapping and dispersion of coral eggs around Bowden reef, great barrier reef, following mass coral spawning. *Continental Shelf Research*, *9*(5), 479–496. https://doi.org/10.1016/0278-4343(89)90011-3

Wolanski, E., & Kingsford, M. J. (2014). Oceanographic and behavioural assumptions in models of the fate of coral and coral reef fish larvae. *Journal of the Royal Society Interface*, *11*(98). https://doi.org/10.1098/rsif.2014.0209

Wood, S., Paris, C. B., Ridgwell, A., & Hendy, E. J. (2014). Modelling dispersal and connectivity of broadcast spawning corals at the global scale. *Global Ecology and Biogeography*, *23*(1), 1–11. https://doi.org/10.1111/geb.12101

Woodruff, S. D., Slutz, R. J., Jenne, R. L., & Steurer, P. M. (1987). A comprehensive ocean-atmosphere data set. *Bulletin of the American Meteorological Society*, *68*(10), 1239–1250. https://doi.org/10.1175/1520-0477(1987)068<1239:ACOADS>2.0.CO;2

Yamano, H., Kayanne, H., Yonekura, N., Nakamura, H., & Kudo, K. (1998). Water circulation in a fringing reef located in a monsoon area: Kabira reef, Ishigaki Island, Southwest Japan. *Coral Reefs*, *17*(1), 89–99. https://doi.org/10.1007/s003380050101

Yuan, Y., Kaneko, A., Su, J., Zhu, X., Liu, Y., Gohda, N., & Chen, H. (1998). The Kuroshio east of Taiwan and in the East China Sea and the currents east of Ryukyu Islands during early summer of 1996. *Journal of Oceanography*, *54*(3), 217–226. https://doi.org/10.1007/BF02751697

Zayasu, Y., Nakajima, Y., Sakai, K., Suzuki, G., Satoh, N., & Shinzato, C. (2016). Unexpectedly complex gradation of coral population structure in the Nansei Islands, Japan. *Ecology and Evolution*, *6*(15), 5491–5505. https://doi.org/10.1002/ece3.2296

Zayasu, Y., & Shinzato, C. (2016). Hope for coral reef rehabilitation: Massive synchronous spawning by outplanted corals in Okinawa, Japan. *Coral Reefs*, *35*(4), 1295. https://doi.org/10.1007/s00338-016-1463-7